Flamelet Modeling for Supersonic Combustion

Tomasz G. Drozda, Jesse R. Quinlan and J. Philip Drummond

Abstract Flamelet models have proven useful in enabling fast and accurate simulations of subsonic turbulent combustion. However, in supersonic combustion, these models face many challenges. The current work presents an a priori analysis of the steady flamelet model using the HIFiRE Direct Connect Rig (HDCR) dual-mode scramjet combustor. The analysis uses Reynolds-averaged simulation (RAS) data obtained with a finite-rate reaction mechanism to assess some of the flamelet model assumptions. Two flight conditions are numerically simulated: Mach 5.84 and Mach 8. These conditions cover a range of combustion phenomena that could be expected to occur in a scramjet engine during flight. The analysis reveals that both nonpremixed and premixed combustion occur in the HDCR combustor. In addition, under some conditions, strong finite-rate effects are also present. These physical aspects could be readily modeled with existing flamelet techniques, however, the effects of variable pressure, wall heat transfer, and flamelet equation boundary conditions are more challenging to address. The latter three elements present the key barriers to utilizing flamelets for supersonic combustion simulations. Although techniques to address these additional challenges are limited, a few perspectives are provided highlighting physics-based requirements in the context of flamelet modeling.

Keywords Flamelet modeling · Combustion modeling · Turbulent reacting flows · Supersonic flows · Reynolds average simulation · HIFiRE 2

1 Introduction

Accurate numerical simulations of supersonic, turbulent, reacting flows present some of the most challenging problems encountered today in fluid mechanics. This is

T. G. Drozda (✉) · J. R. Quinlan · J. P. Drummond
NASA Langley Research Center, Hampton, VA 23666, USA
e-mail: tomasz.g.drozda@nasa.gov

J. R. Quinlan
e-mail: jesse.r.quinlan@nasa.gov

J. P. Drummond
e-mail: j.p.drummond@nasa.gov

because, unlike subsonic combustors, supersonic combustors contain complex and coupled interactions of compressible flow features, such as shocks and expansions, with other elements of the flow like laminar, transitional, and turbulent boundary layers, turbulence itself, mixing-layers, large-scale vorticity, and combustion. These nonlinear interactions can drastically alter the flow behavior and lead to: shock-induced flow transition and/or separation, which change the effective flow area and alter the shock structure in the combustor; shock-turbulence interactions, which can amplify turbulence intensity; shock-mixing-layer interactions, which introduce baroclinic torque that can change fuel-air mixing and therefore rates of chemical reactions; and strong flow-chemistry coupling, which is responsible for potentially significant and rapid pressure rise due to the heat release. Furthermore, unlike subsonic combustors, which are typically designed with a specific combustion mode in mind, supersonic combustors often exhibit regions of nonpremixed, partially premixed, and premixed combustion. This is because low combustor temperatures and pressures increase ignition delay time, while at the same time, fast flow through times decrease residence times. Both effects result in partial premixing of the fuel and air in a high-speed combustor. In addition, flameholding devices utilize areas of flow recirculation that may contain fully and/or partially premixed burning fuel-air mixtures. All of these difficult to model and simulate flow elements are compounded onto the challenges of subsonic combustion, which includes turbulence and turbulence-chemistry interaction modeling, radiation modeling, and chemical kinetics modeling. As a final challenge of supersonic combustion, it should be noted that, unlike their subsonic counterparts, supersonic combustors are typically an order of magnitude larger in length and cross section area, operate at higher Reynolds numbers, and are highly integrated into the vehicle airframe [1]. Because of the above challenges, numerical simulations of supersonic combustors typically require an order-of-magnitude or more dynamic range of scales and therefore more computational resources (i.e., grid points). One aspect of supersonic flow simulations that is simpler than that of subsonic simulations is the specification of the boundary conditions [2], e.g., a supersonic inflow boundary does not exhibit an outward-traveling characteristic, and a supersonic outflow does not exhibit an inward-traveling characteristic. By contrast, subsonic flow typically requires physically consistent treatment of the outgoing and incoming flow characteristics [2] to ensure that simulations are well-posed, stable, and accurate.

The computational resources needed for reacting simulations also rapidly increase with the number of species transport equations and chemical reactions that must be solved for a given chemical kinetics model, which depend on the complexity of the fuel. A typical chemical kinetics model for even a simple fuel like hydrogen can have 9 species and 19 reactions [3], which more than doubles the number of solved transport equations for a three-dimensional Reynolds-averaged simulation (RAS) of a turbulent flow with a 2-equation turbulence model [4] typically used in practice. Chemical kinetics models for complex hydrocarbon fuels can contain 1,000s of species and 10,000s of chemical reactions [5] making numerical simulations all but intractable except for simple zero- and one-dimensional flame simulation configurations [6, 7]. For these reasons, the vast majority of computational simulations of

turbulent supersonic combustion have relied on only the most simplified or reduced mechanisms [8, 9] and/or phenomenological models of combustion [10], both of which limit predictive capability. In addition to increasing the number of needed equations, reaction rate constants found in most chemical kinetics models follow the Arrhenius form, which is expensive to evaluate numerically and introduces numerical stiffness, thereby further increasing the simulation time.

For numerical simulations to accurately and effectively contribute to the engineering design process, the simulation times must be kept to a minimum. Because chemical kinetics have such a strong influence on the overall simulation cost, often increasing it by an order of magnitude or more as compared to the corresponding nonreacting simulation, it is natural to seek models that reduce the number of needed species transport equations while simultaneously maintaining, to the extent possible, the fidelity of a complex chemical kinetics model. In general, the basis for the reduction hinges on the assumptions about the important chemical reactions [11] and/or the state of the underlying combustion physics. The laminar flamelet model introduced by Peters [12–14] follows the latter and assumes that local combustion processes progress much faster than those corresponding to the bulk flow motions that tend to strain and extinguish the local flame. Conceptually, this leads to a thin flame or a reaction front (called a flamelet) that is convected, distorted, and wrinkled by the otherwise nonreacting, often turbulent, flowfield [15, 16]. Although this flowfield is capable of warping the thin flame that it is convecting, it does not significantly alter the internal structure of the flame. Therefore, under the flamelet model, only the flow gradients in a single dimension normal to the flame can influence the local reaction chemistry. Consequently, complex three-dimensional (3D), wrinkled, turbulent flames may be approximated using an ensemble of local one-dimensional (1D), laminar flames. This phenomenology effectively allows the 1D laminar flame and its underlying chemical kinetics to be decoupled from the flowfield and solved independently using a set of simplified partial differential equations called the flamelet equations. The flamelet equations are derived from the conservation equations for the species mass, momentum, and energy (i.e., Navier-Stokes with species transport) by transforming the spatial coordinates into a coordinate normal to the flame surface and simplifying [17] or by utilizing a Crocco-type transformation to transform the spatial coordinate into a state-space variable called a mixture fraction [12, 14]. The fundamental property of the mixture fraction is that it is a nonreacting (passive) scalar quantity that can be used to track the local state of the mixture because it represents a fraction of mass that originated in the fuel stream. The mixture fraction is also the key element of the flamelet model because it parameterizes, independently of the type of fuel used, the complete thermochemical state of the flame by a single scalar quantity. This allows the flamelet model to retain many elements of the realistic chemistry and significantly reduces the computational costs of reacting simulations, especially for complex hydrocarbon fuels. Indeed, the laminar flamelet model was developed to enable any combustion simulation, at a time when the available computational resources were prohibitively limited. Currently, the laminar flamelet models continue to be useful by enabling practical combustion simulations with large eddy

simulations (LES) [18, 19] and optimization and uncertainty quantification studies with RAS [20].

Conventional flamelet modeling typically involves a tabulation step that provides relationships between the mixture fraction and the rest of the thermochemical state-space. This tabulation may be performed as a simulation preprocessing step or in situ [21]. The flamelet model may further be augmented by the assumed probability density function (PDF) turbulence-chemistry interaction (TCI) model [22–25] whose contribution can be included in the flamelet table. Including the assumed PDF model in the flamelet table requires an additional lookup parameter, typically mixture fraction variance, that identifies the level of turbulence intensity in the TCI model. The resulting lookup table contains all the species and thermodynamic state variables over the range of turbulence intensities needed to execute the simulation, and completely eliminates the need to computationally evaluate expensive reaction rates during the simulation, which also results in the removal of numerical stiffness associated with the Arrhenius reactions rate constants.

In practice, to generate a flamelet lookup table, the flamelet equations must be solved subject to certain boundary conditions. These boundary conditions specify the mixture composition of the fuel and oxidizer streams, and their respective temperatures. In addition, a constant value of the pressure experienced by the flame is needed as well as an equation of state, e.g., the ideal gas law. The characteristic strain imposed by the flowfield on the flame is also needed. For the flamelet equations transformed into the flame-normal coordinate, the "strain" is provided by specifying the 1D computational domain length, and fuel and oxidizer stream velocities normal to the flame. For the flamelet equations transformed into the mixture fraction state-space, the flame strain is replaced by the scalar dissipation rate. The strain and scalar dissipation rate are important parameters because they control the extent to which the 1D laminar flame can burn. Small strain leads to near-equilibrium combustion, whereas large strain can lead to a fully extinguished mixing solution. Therefore, to fully encompass the range of potential flamelet states, the strain rate or scalar dissipation rate can be included as an additional independent table parameter. However, the strain and the scalar dissipation rate are not directly related to the combustion process and lead to multivalued parameterization of the combustion state-space. To overcome this issue, either one of these quantities can be replaced in the flamelet table by a progress variable [26], which is usually a linear combination of one or more combustion product species [27]. Unlike the mixture fraction, the progress variable cannot be a passive scalar because it must be able to track the progress of combustion from near-equilibrium conditions to flame extinction and vice versa. In addition, the specific definition of the progress variable, together with the mixture fraction, must offer a unique mapping of the combustion state-space [27].

The above narrative describes the most computationally efficient steady laminar flamelet (SLF) model, where the word steady indicates that the flamelet equations have been integrated to steady-state and those results tabulated. The key limitations of this model are the inability to treat partially-premixed or premixed combustion systems, and for nonpremixed systems, the inability to model multifuel or multioxidizer streams with different stream temperatures or at different pressures. In

addition, the SLF model cannot accurately capture autoignition processes [28] nor heat transfer effects to the combustor walls. Despite the attractive and significant computational cost savings, the limitations of the SLF model significantly narrow, in theory, its range of practical applicability. Nevertheless, flamelet models, in general, have often been found to perform acceptably even for cases that are a priori known to violate some of the theoretical bounds of the model. This may be because flow regions containing unsupported physics do not drive the leading flow behavior for a particular case or that some limitations are not as restrictive as others. For example, the requirement of constant pressure is of no consequence for subsonic combustion where pressure variations within a combustor are small or at hypervelocity Mach numbers, where the heat release does not significantly raise the combustor pressure. Even pressure variations by a factor of 2 only produce reaction rate changes of the order 4, which may be within the error bound of a typical chemical kinetics model. However, other limitations may be critical; for example, in multiphase fuel spray combustion systems, the temperature of the gaseous oxidizer surrounding the evaporating liquid fuel droplet increases as the evaporated fuel mixes and reacts with the oxidizer. Modeling the latter process with steady flamelet equations would require (at the least) a variable oxidizer boundary condition, whose range is difficult to estimate a priori. Nevertheless, many of the limitations of the steady flamelet model have been addressed, albeit often at the expense of increased computational cost, by several new classes of the flamelet approach, namely: the unsteady flamelet model (also known as the representative interactive flamelet (RIF) model) [28–30], the flamelet progress variable (FPV) model [26, 31, 32], and the flamelet-generated manifolds (FGM) model [33–35].

In supersonic combustion, three physical effects complicate the formulation and implementation of the flamelet model. The first is the heat-release-induced pressure rise, which increases the pressure experienced by the flame as the reactions progress, thereby altering the chemical kinetics. The second is the viscous heating, which increases local mixing-layer and boundary layer temperatures and at higher Mach numbers may lead to oxidizer and fuel dissociation via endothermic reactions, processes that are not included in the flamelet equations. These two effects are important at opposite ends of the flight Mach number range; that is, for flight Mach numbers up to about 6–8, the heat-release-induced pressure rise is significant but its importance begins to decrease as the flight Mach number begins to exceed 10–12. The opposite is true for viscous heating, which is not significant compared to the heat release at Mach numbers less than about 4, but can lead to dissociation at Mach numbers in excess of about 7–8. Viscous heating is also much more difficult to account for using the flamelet methodology because it represents physical processes that are typically explicitly excluded from the energy equation when deriving the flamelet equations. Nevertheless, these effects could be qualitatively incorporated into the tabulation process or the unsteady flamelet model by allowing variations in the flamelet boundary conditions (e.g., temperature and composition of fuel and oxidizer streams). The third physical effect is the significant heat transfer that could occur to the combustor walls. For both supersonic and subsonic combustors, heat transfer to the wall is a result of flame-wall interactions and combustion products

being convected and/or diffused toward the cold walls. In addition, for high Mach number supersonic combustors, the heat transfer is also the result of viscous heating of the near-wall mixture. This mixture could contain pure fuel or pure air, or a burned or unburned mixture of the two. In all cases, the cooling process results in the decrease in the enthalpy of the mixture to states not accounted for in the flamelet table.

To demonstrate the extent of the applicability of the flamelet model to supersonic combustion, the Hypersonic International Flight Research Experimentation (HIFiRE) Direct Connect Rig (HDCR) [36, 37] dual-mode supersonic combustion ramjet (scramjet) combustor is used in this work. To accomplish this, 3D RAS are performed of the HDCR geometry using a 22-species finite-rate reduced reaction mechanism for a JP-7 fuel surrogate [38]. Although designed for academic and collaborative purposes, the HDCR is representative of a practical cavity-stabilized scramjet combustor. TCI modeling is omitted in the current work to focus the analysis on the flamelet model performance rather than the coupled performance of the flamelet and TCI models. Two HDCR flight conditions are analyzed: a Mach 5.84 dual-mode supersonic combustion mode, which exhibits both subsonic and supersonic combustion regions; and a Mach 8 scramjet mode, which consists of primarily supersonic combustion. Both flight conditions are analyzed to characterize the fundamental nature of the combustion. The current combustion mode analysis may not reveal the true nature of all combustion modes potentially present in the HDCR because modeling errors introduced by the turbulence and chemical kinetics models and the absence of various other physics submodels (e.g., TCI model), nevertheless, previous work [39] showed that the current simulations correctly reproduce the experimentally obtained HDCR combustor pressure rise and therefore heat release distribution.

This chapter is organized as follows. First, the governing equations applicable to high-speed compressible turbulent reacting flows are introduced, followed by the concept of the mixture fraction and its transport equation, the flamelet equations, and the progress variable. Second, some of the phenomenology observed in supersonic combustion is described and combustion mode analysis is utilized to identify the range of relevant phenomena present in the HDCR simulations. Third, the challenges of accounting for the variable pressure, wall heat transfer, and changing flamelet equation boundary conditions are discussed. The chapter concludes by discussing some of the challenges that continue to face the flamelet modeling approach in supersonic combustion.

2 Governing Equations

The details of the derivation of the transport equations governing fluid flows in thermodynamic equilibrium are documented in many undergraduate and graduate texts [2, 40–45] and will not be repeated here. Flows in thermodynamic non-equilibrium and multiphase flows are not considered, but common practical

approaches to treating these flows are discussed by Gnoffo et al. [46], Park [47] and Faeth [48]. The derivations of the governing equations for the motion of a fluid in thermodynamic equilibrium lead to a set of elegant nonlinear partial differential equations (PDEs) governing the transport of several conserved quantities: species mass, momentum, and energy. One of the earliest complete discussions of these equations with an application to high speed reacting flows is offered by Drummond [49]. These equations can also be further manipulated to obtain other transport equations for quantities such as vorticity, enthalpy, or (combining with the second law of thermodynamics) entropy that have been found useful in elucidating physical behaviors of flows [50].

The governing conservation equations encompass a wide range of physical fluid flow phenomena. One particularly complex phenomena is that of a turbulent flow. The discussion of turbulence physics is beyond the scope of this text, but several excellent texts are available [51–54] with many more describing computational [2, 49, 55–60] and modeling [61–65] treatments. Nevertheless, a few words relevant to the current discussion are warranted. Foremost, it should be stated that one characteristic of turbulent flows, which is responsible for the difficulty encountered in theoretical and numerical analysis, is the multiscale nature of turbulence. That is, the fluid motions in a turbulent flow occur over a wide range of both time and length scales with the ratio of large to small turbulence flow scales proportional to the 3/4 power of the Reynolds number [54]. For a problem of practical interest, this leads to the required number of computational cells for direct numerical simulation (DNS) to be on the order of $1 - 10 \times 10^9$ (i.e., three orders of magnitude in each of the three spatial dimensions). By contrast, the grid resolutions that are used in simulations of practical interest on capacity cluster hardware and in the amount of time required to make a programmatic impact are typically on the order of $10 - 100 \times 10^6$. That is, the typical current capability for numerical simulations of turbulent flows is almost two to three orders of magnitude smaller than that required for the corresponding direct simulations. Therefore, even before the flamelet model is introduced to reduce the computational cost of combustion, any numerical simulation involving turbulent flow must be set up to utilize the existing computer hardware in a reasonable amount of time and still be able to investigate and analyze turbulent reacting flows of interest.

One approach is to reduce the effective dynamic range of turbulent length and time scales to that which can be reasonably considered for simulations on a current computer. Unfortunately, this constrains the simulations to only a portion of the turbulence length scales with the removed portions requiring a mathematical model for the effects they have on those being simulated. This is called the closure problem and such modeling has been a topic of research for the past century [66] with significant developments in the last 50 years. In the current work, a common form of the governing conservation equations are presented. These equations can be obtained by either time-averaging (or ensemble-averaging) [62] to derive transport equations used for RAS, or spatial-averaging (or filtering) [63] to derive the LES equations. Despite the very different approach of these two methods to the turbulence scale reduction, the mathematical operations of time-averaging and spatial-averaging produce the exact same set of transport equations. What differs are the interpretations of

the terms, their closures, and the numerical implementation requirements, with the spatially-averaged transport equations for LES typically requiring unsteady, high-order accurate numerical schemes to properly resolve the turbulence length scales near the filter scale.

In what follows, the nondimensional form of the Favré-averaged transport equations are presented. These equations arise as a result of applying the time-average operator to the governing transport equations. The time-average and Favré-average of an arbitrary quantity, f, are denoted by an $\overline{f}$ and $\widetilde{f}$, respectively, and they are related to each other via the density, i.e., $\overline{\rho}\widetilde{f} = \overline{\rho f}$. The resulting Favré-averaged equations are commonly used to perform RAS of high-speed, turbulent, reacting flows. Applying the Favré-averaging operator to the governing equations for mass, species mass fractions, momentum, and energy results in:

$$\frac{\partial\overline{\rho}}{\partial t} + \frac{\partial\overline{\rho}\widetilde{u}_k}{\partial x_k} = 0, \tag{1}$$

$$\frac{\partial\overline{\rho}\widetilde{Y}_\alpha}{\partial t} + \frac{\partial\overline{\rho}(\widetilde{u}_k + \widehat{V}_k^c)\widetilde{Y}_\alpha}{\partial x_k} = \frac{\partial}{\partial x_k}\left(\frac{\widehat{\mu}}{\widehat{Sc}_\alpha}\frac{\partial\widetilde{Y}_\alpha}{\partial x_k}\right) + \dot{\omega}_\alpha(\overline{p}, \widetilde{Y}_\alpha, \widetilde{T})$$
$$- \underbrace{\frac{\partial}{\partial x_k}\left(\overline{\widetilde{\rho u_k Y_\alpha}} - \overline{\rho}\widetilde{u}_k\widetilde{Y}_\alpha\right)}_{\text{Turbulence Flux}} + \underbrace{\left(\overline{\dot{\omega}_\alpha(p, Y_\alpha, T)} - \dot{\omega}_\alpha(\overline{p}, \widetilde{Y}_\alpha, \widetilde{T})\right)}_{\text{Turbulence Chemistry Interaction (TCI)}},$$
$$\alpha = 1, 2, \ldots, N, \tag{2}$$

$$\frac{\partial\overline{\rho}\widetilde{u}_i}{\partial t} + \frac{\partial\overline{\rho}\widetilde{u}_k\widetilde{u}_i}{\partial x_k} = -\frac{\partial\overline{p}}{\partial x_i} + \frac{M_r}{Re_r}\frac{\partial}{\partial x_k}\left(\widehat{\mu}\left(\frac{\partial\widetilde{u}_i}{\partial x_k} + \frac{\partial\widetilde{u}_k}{\partial x_i}\right) - \frac{2}{3}\widehat{\mu}\frac{\partial\widetilde{u}_j}{\partial x_j}\delta_{ik}\right)$$
$$- \underbrace{\frac{\partial}{\partial x_k}\left(\overline{\widetilde{\rho u_k u_i}} - \overline{\rho}\widetilde{u}_k\widetilde{u}_i\right)}_{\text{Turbulence Stress}}, \tag{3}$$

$$\frac{\partial\overline{\rho}\widetilde{e^t}}{\partial t} + \frac{\partial\overline{\rho}(\widetilde{u}_k + \widehat{V}_k^c)\widetilde{h^t}}{\partial x_k} = \frac{M_r}{Re_r}\frac{\partial}{\partial x_k}\left(\widetilde{u}_i\left(\widehat{\mu}\left(\frac{\partial\widetilde{u}_i}{\partial x_k} + \frac{\partial\widetilde{u}_k}{\partial x_i}\right) - \frac{2}{3}\widehat{\mu}\frac{\partial\widetilde{u}_j}{\partial x_j}\delta_{ik}\right)\right)$$
$$+ \underbrace{\frac{M_r}{Re_r}\frac{\partial}{\partial x_k}\left(\overline{u_i\tau_{ik}} - \widetilde{u}_k\overline{\tau_{ik}}\right)}_{\text{Velocity-Shear Stress Correlation}} + \frac{M_r}{Re_r Pr_r}\frac{\partial}{\partial x_k}\left(\frac{\widehat{\mu}}{\widehat{Pr}}\frac{\partial\widetilde{h}}{\partial x_k} - \frac{\widehat{\mu}}{\widehat{Pr}}\sum_\alpha\left(\frac{\widehat{Le}_\alpha - 1}{\widehat{Le}_\alpha}\right)\widetilde{h}_\alpha\frac{\partial\widetilde{Y}_\alpha}{\partial x_k}\right)$$
$$+ \frac{\partial\overline{\rho}(\widetilde{k} + k)\widehat{V}_k^c}{\partial x_k} - \underbrace{\frac{\partial}{\partial x_k}\left(\overline{\widetilde{\rho u_k h}} - \overline{\rho}\widetilde{u}_k\widetilde{h}\right)}_{\text{Turbulence Enthalpy Flux}} - \underbrace{\frac{\partial}{\partial x_k}\left(\overline{\rho u_k \frac{\widetilde{u_i u_i}}{2}} - \overline{\rho}\widetilde{u}_k\frac{\widetilde{u_i u_i}}{2}\right)}_{\text{Turbulent Kinetic Energy Flux}}, \tag{4}$$

where ρ, Y_α, u_i, V_k^c, e^t, h^t, h, h_α, k, p, T, μ, τ_{ij}, and $\dot{\omega}_\alpha$ are the density, mass fraction of species α, velocity, differential diffusion correction velocity, total energy, total enthalpy, enthalpy, enthalpy of species α, kinetic energy, pressure, temperature, mixture molecular viscosity, shear-stress, and reaction rate of species α, respectively. Temporal and spatial coordinates are denoted by t, and x_i. The equations are also nondimensionalized with M_r, Re_r, Pr_r, denoting reference Mach, Reynolds, and Prandtl numbers, respectively. Pr, Sc_α, and Le_α are the mixture Prandtl number, and the Schmidt and Lewis numbers for species α. In addition, the "hat" over an arbitrary quantity, $\widehat{f}$, denotes a nonlinear function quantity evaluated using the Favré averaged variables, for example,

$$\widehat{V_k^c} = \sum_\alpha \frac{\widehat{\mu}}{\widehat{Sc}_\alpha} \frac{\partial \widetilde{Y}_\alpha}{\partial x_k}, \ \widehat{\mu} = \mu(\widehat{T}), \ \widehat{Sc}_\alpha = \frac{\widehat{\mu}}{\overline{\rho}\widehat{D}_\alpha}. \tag{5}$$

It should be noted that the mixture Pr, Sc_α, and Le_α quantities in Eqs. (2), and (4) are denoted with a "hat" because, although they could be constants, in general, they are nonlinear functions of both the thermodynamic and transport properties of the mixture. In addition, the temperature is also denoted with the "hat" because, for noncalorically perfect gases, it is obtained by iteration from the Favré averaged mixture enthalpy. Furthermore, it should also be noted that when the species diffusivities are all equal, i.e., $Sc_\alpha = Sc$, then the differential diffusion correction velocity, $\widehat{V_k^c}$ is identically zero. This assumption is commonly used when simulating turbulent reacting flows.

The various forms of energies are related by the first law of thermodynamics,

$$\widetilde{e^t} = \widetilde{e} + \widetilde{k} + k, \ \widetilde{h^t} = \widetilde{h} + \widetilde{k} + k,$$
$$\widetilde{k} = \frac{1}{2}\widetilde{u}_i\widetilde{u}_i, \ k = \frac{1}{2}\left(\widetilde{u_i u_i} - \widetilde{u}_i\widetilde{u}_i\right), \tag{6}$$

where e is the internal energy.

All of the terms within the underbraces in Eqs. (1–4) and the turbulent kinetic energy are unclosed and must be modeled. The above equations further require a time-averaged form of the equation of state, which for an ideal gas becomes,

$$\overline{p} = \overline{\rho}\widetilde{R}\widetilde{T} = \overline{\rho}\sum_\alpha \frac{Ru}{W_\alpha}\widetilde{Y}_\alpha\widetilde{T} + \underbrace{\overline{\rho}\sum_\alpha \frac{Ru}{W_\alpha}(\widetilde{Y_\alpha T} - \widetilde{Y}_\alpha\widetilde{T})}_{\text{Scalar-Temperature Correlation}}, \tag{7}$$

where R, R_u, and W_α are the mixture gas constant, universal gas constant, and molecular weight of species α, respectively. The unclosed scalar-temperature correlation term is most commonly neglected. Further discussion on modeling the unclosed terms for practical high-speed applications for RAS is offered by Baurle [67].

2.1 Mixture Fraction

All flamelet models rely on the mixture fraction as a means of parameterizing combustion physics. By definition, the mixture fraction represents a mass fraction of all material that originated in the fuel stream that is present locally in the mixture. The formal definition of the mixture fraction can be written as:

$$Z = \frac{\beta - \beta_O}{\beta_F - \beta_O} \tag{8}$$

where Z is the mixture fraction and β_F and β_O are the mass fractions of the fuel material in the fuel and oxidizer streams, respectively. The definition of β is:

$$\beta = \sum_i \gamma_i Z_i = \sum_i \gamma_i \sum_j \frac{a_{ij} W_i Y_j}{W_j}, \quad i = C, H, O, \quad j = 1, 2, \ldots, N, \tag{9}$$

where γ_i is a weight corresponding to each element present in the mixture, Z_i is elemental mass fraction (e.g. Z_C, Z_H, Z_O), a_{ij} is the number of atoms of element i in species j. It is clear from Eq. (8) that the mixture fraction takes values in the range of 0 to 1, which correspond to pure oxidizer and fuel streams, respectively. Equation (9) also shows that the mixture fraction is a linear combination of elemental mass fractions. By conservation of mass, the latter are conserved scalars, therefore, the mixture fraction must be a conserved scalar also. Specific values of γ_i define a particular mixture fraction. Table 1 shows commonly used definitions. The mixture fraction can also be used to calculate the fuel-to-oxidizer mass ratio. Since by definition, the mixture fraction represents the mass fraction of elements originating in the fuel stream, the fuel-to-oxidizer mass ratio becomes,

Table 1 Elemental mixture fraction weights

γ_C	γ_H	γ_O	Notes
$\frac{2}{W_C}$	$\frac{1}{2W_H}$	$-\frac{1}{W_O}$	Bilger's definition [68]
$\frac{2}{W_C}$	$\frac{1}{2W_H}$	0	Barlow's definition (for Sandia Flames) [69]
1	0	0	Elemental mixture fraction for C
0	1	0	Elemental mixture fraction for H

$$\frac{F}{O} = \frac{Z}{1 - Z},$$

(10)

where $1 - Z$ is the mass fraction of material in the mixture that originated in the oxidizer stream. When the oxidizer is air, Eq. (10) represents the fuel-to-air ratio. The fuel equivalence ratio can also be computed by dividing the fuel-to-air ratio by its value evaluated at the stoichiometric value of the mixture fraction.

The mixture fraction transport equation is derived by applying the definition of the mixture fraction, Eqs. (8) and (9), to the unaveraged transport equations for the mass fractions. The result is;

$$\frac{\partial \rho Z}{\partial t} + \frac{\partial \rho u_i Z}{\partial x_i} = \frac{\partial}{\partial x_i} \left(\frac{\mu}{Sc} \frac{\partial Z}{\partial x_i} \right) + \epsilon_{DD},$$

(11)

where the source term ϵ_{DD} is a correction factor due to the differential diffusion (DD) [70],

$$\epsilon_{DD} = \frac{1}{\beta_F - \beta_O} \sum_n \gamma_n \sum_\alpha \frac{a_{n\alpha} W_n}{W_\alpha} \frac{\partial J_{\alpha i}}{\partial x_i} - \frac{\partial}{\partial x_i} \left(\frac{\mu}{Sc} \frac{\partial Z}{\partial x_i} \right),$$

(12)

where $J_{\alpha i}$ is the diffusive flux of species α in the i-th direction. Most commonly, the mixture fraction transport equation is derived assuming equal diffusivities among the species in the mixture, i.e., $J_{\alpha i} = J_i$. Under this assumption ϵ_{DD} is identically zero. Assuming equal diffusivities and applying time averaging operator to Eq. (11) yields,

$$\frac{\partial \overline{\rho} \widetilde{Z}}{\partial t} + \frac{\partial \overline{\rho} \widetilde{u}_i \widetilde{Z}}{\partial x_i} = \frac{\partial}{\partial x_i} \left(\frac{\widehat{\mu}}{\widehat{Sc}} \frac{\partial \widetilde{Z}}{\partial x_i} \right) - \underbrace{\frac{\partial}{\partial x_k} \left(\overline{\rho u_k Z} - \overline{\rho} \widetilde{u}_k \widetilde{Z} \right)}_{\text{Turbulence Flux}},$$

(13)

where the term inside the underbrace is the unclosed turbulence mixture fraction flux and must be modeled.

Many TCI models, including presumed and transport PDF models, utilize the mixture fraction variance as a key aggregate variable by which to quantify the turbulence intensity experienced by the species. The mixture fraction variance is defined as,

$$\widetilde{Z''^2} = \widetilde{Z^2} - \widetilde{Z}^2.$$

(14)

The transport equation for this quantity can be readily obtained by subtracting the transport equation for $\widetilde{Z}^2$ from the transport equation for $\widetilde{Z^2}$, both of which can be derived in a manner similar to that used to obtain Eq. (13). The result is,

$$\frac{\partial \overline{\rho} \widetilde{Z''^2}}{\partial t} + \frac{\partial \overline{\rho} \widetilde{u_i} \widetilde{Z''^2}}{\partial x_i} = \frac{\partial}{\partial x_i} \left(\frac{\widehat{\mu}}{\widehat{Sc}} \frac{\partial \widetilde{Z''^2}}{\partial x_i} \right) - 2 \underbrace{\left(\overline{\rho u_i Z} - \overline{\rho} \widetilde{u_i} \widetilde{Z} \right)}_{\text{Turbulence Flux}} \frac{\partial \widetilde{Z}}{\partial x_i}$$

$$- 2 \frac{\widehat{\mu}}{\widehat{Sc}} \underbrace{\left(\overline{\frac{\partial Z}{\partial x_i} \frac{\partial Z}{\partial x_i}} - \frac{\partial \widetilde{Z}}{\partial x_i} \frac{\partial \widetilde{Z}}{\partial x_i} \right)}_{\text{Dissipation}} - \frac{\partial}{\partial x_i} \underbrace{\left(\overline{\rho} \left(\widetilde{u_i Z^2} - \widetilde{u_i} \widetilde{Z^2} \right) - 2 \overline{\rho} \widetilde{Z} \left(\widetilde{u_i Z} - \widetilde{u_i} \widetilde{Z} \right) \right)}_{\text{Turbulence Transport}} .$$

$$(15)$$

The terms on the right hand side represent molecular diffusion, production, dissipation, and turbulent transport, respectively, of the mixture fraction variance.

2.2 Flamelet Equations

Several approaches have been used to obtain flamelet manifolds for both non-premixed and premixed flames [26, 33]. All approaches involve solutions to the one-dimensional forms of partial differential equations that result from transforming the governing equations for mass, momentum, and energy into a flame adapted coordinate system. The original approach proposed by Peters [12], utilizes a Crocco-type transformation from spatial coordinates to the mixture fraction coordinate. Applying this transformation to the unaveraged transport equations for species mass fractions and energy produces a set of laminar flamelet equations,

$$\rho \frac{\partial Y_\alpha}{\partial t} = \frac{1}{2} \rho \chi_\alpha \frac{\partial^2 Y_\alpha}{\partial Z^2} + \dot{\omega}_\alpha, \tag{16}$$

$$\rho \frac{\partial h}{\partial t} = \frac{1}{2} \rho \chi \frac{\partial^2 h}{\partial Z^2} \tag{17}$$

where χ_α, and χ are the scalar dissipation for species α, and scalar dissipation for the mixture, respectively. The scalar dissipations are defined as,

$$\chi_\alpha = 2 \frac{\mu}{\rho Sc_\alpha} \frac{\partial Z}{\partial x_j} \frac{\partial Z}{\partial x_j}, \ \chi = 2 \frac{\mu}{\rho Sc} \frac{\partial Z}{\partial x_j} \frac{\partial Z}{\partial x_j}. \tag{18}$$

It should be noted that the above equations account for the effect of differential diffusion and should be solved together with Eq. (11) containing a model for ϵ_{DD}. However, by assuming unity Lewis number, which also leads to constant values for Sc_α, a more common form of the flamelet equations that neglects the effect of differential diffusion is obtained. It should further be noted that the above flamelet equationsare derived using a low-Mach-number approximation form of the energy

equation, where the first term on the right hand side of Eq. (4) is neglected. As a consequence, the viscous heating effects, which may be important in high-speed flows, are not captured by the flamelet manifold obtained using Eqs. (16) and (17).

Equations (16) and (17) represent a boundary-value problem that can be solved by specifying the species composition and temperature for the fuel ($Z = 1$) and oxidizer ($Z = 0$) streams, and the pressure for the mixture. Although in high-speed flows the pressure can vary between fuel and oxidizer streams, this effect cannot be captured by the flamelet equations, however for thin flames, this variation can be neglected. The scalar dissipation rates must also be specified. For RAS, a few models for these quantities can be obtained following the analogy to the dissipation of turbulent kinetic energy [2], which results in the scalar dissipation rate being a function of the turbulence dissipation, turbulent kinetic energy, and the mixture fraction variance. Because mixture fraction is bounded between 0 and 1, for a given value of the mixture fraction, there exists a theoretical upper limit of the mixture fraction variance, which limits the scalar dissipation rate.

The scalar dissipation rate controls the extent to which the flame is burning. For χ values approaching zero, a near-equilibrium chemistry solution is obtained, whereas for values approaching infinity, the nonreacting solution is recovered. The intermediate flamelet solutions can be obtained by varying the value of the scalar dissipation rate within those limits. However, care must be taken when attempting to generate a sequence of flamelet manifolds in this way because there exist three distinct flamelet solutions, corresponding to nonreacting, unstable burning, and stable burning, for a single value of the scalar dissipation rate. This multivalued nature of the scalar dissipation requires special simulation approaches [71, 72] to obtain all possible solutions. This also complicates the scalar dissipation's role as a parameterizing quantity, which requires a unique parameterization of the thermochemical state for applications. For this reason, early applications omitted the unstable flamelet branch from the flamelet table. More recently, a progress variable quantity [26, 31] has been introduced to improve unique parameterization of all possible flamelet solutions.

2.3   Progress Variable Equation

Instead of using Z and χ to parameterize solutions of the flamelet equations, a progress variable, C, is introduced to replace the latter. The progress variable is defined such that it provides a correlation with the global progress of the combustion and is typically a linear combination of combustion-product species mass fractions. For example, Pierce and Moin [31] have proposed $C = Y_{CO_2} + Y_{H_2O}$ for hydrocarbon fuels. Unlike the mixture fraction, the progress variable is a reacting scalar. The progress variable is also typically normalized across all manifolds by its equilibrium value, such that $C = 1$ for equilibrium combustion [27]. For nonreacting solutions, $C = 0$. Most importantly, since C is defined to correlate with the reaction's progress, Z and C have the potential to uniquely parameterize all of the flamelet solutions. It should be noted, however, that because of the nonlinear nature of chemical kinet-

ics, the use of the progress variable does not guarantee a unique parameterization, and some limited nonuniqueness typically still exists. Any nonunique regions of the complete flamelet manifold must be "trimmed" to avoid spurious behaviors in applications. Alternately, Ihme et al. [27] have proposed a regularization technique that strives to enforce a unique parameterization of the progress variable, to the extent possible, by introducing and adjusting the weights of the mass fractions that compose the progress variable.

The application of the flamelet model parameterized using Z and C in a computational fluid dynamics (CFD) solver requires a solution of the time-averaged progress variable transport equation along with the transport equation for $\widetilde{Z}$, Eq. (13). Once the definition of the progress variable has been established, the transport equation can be readily derived and generally takes on the form;

$$\frac{\partial \overline{\rho}\widetilde{C}}{\partial t} + \frac{\partial \overline{\rho}\widetilde{u_i}\widetilde{C}}{\partial x_i} = \frac{\partial}{\partial x_i}\left(\frac{\widehat{\mu}}{\widehat{Sc}}\frac{\partial \widetilde{C}}{\partial x_i}\right) - \underbrace{\frac{\partial}{\partial x_k}\left(\widetilde{\overline{\rho u_k C}} - \overline{\rho}\widetilde{u_k}\widetilde{C}\right)}_{\text{Turbulence Flux}}$$
$$+ \dot{\omega}_C(\overline{p}, \widetilde{Z}, \widetilde{C}, \widetilde{T}) + \underbrace{\left(\overline{\dot{\omega}_C(p, Z, C, T)} - \dot{\omega}_C(\overline{p}, \widetilde{Z}, \widetilde{C}, \widetilde{T})\right)}_{\text{Turbulence Chemistry Interaction (TCI)}}, \quad (19)$$

where the terms inside the underbrace are unclosed and must be modeled. It should be noted that, in addition to the unclosed turbulence flux term, which can be modeled in conventional ways, the above transport equation includes an unclosed term for the turbulence and progress variable chemistry interactions. This term is analogous to the TCI term in Eq. (2) and is difficult to model and often simply neglected. The reaction source term, $\dot{\omega}_C$, is evaluated from the solution of the flamelet equations and added to the flamelet table.

3 Introduction to Supersonic Combustion

Supersonic combustion is defined as the conversion of reactants into products that takes place in the supersonic "background" flow. By this definition, a conventional ramjet engine, although capable of supersonic propulsion, does not exhibit supersonic combustion because the supersonic freestream air is compressed and slowed to subsonic speeds prior to injecting the fuel and energizing the engine via combustion. The subsonically-convected combustion products are then expanded to supersonic speeds through the converging-diverging (CD) thrust nozzle. In a ramjet engine, the combustion processes are quite similar to those found in a conventional gas turbine combustors, although the mechanics of compression, fuel injection and mixing, and expansion to produce thrust are different. Supersonic combustion typically occurs in a scramjet engine, where the high-speed freestream air is compressed in such a way that it still remains supersonic when entering the high-speed combustor. One marked

difference between subsonic and supersonic combustion is that the static pressure in the combustor decreases by a few percentage points in a subsonic combustor, whereas it can rise by an order of magnitude in the supersonic combustor. This characteristic pressure rise is a result of the chemical conversion of reactants to products under compressibility effects of a supersonic flow, and is conceptually similar to a Rayleigh flow, i.e., a supersonic model flow with heat addition. However, it should be noted that unlike Rayleigh flow, the total enthalpy of a reacting flow does not change due to combustion and can only be altered by heat addition (or cooling) through the combustor walls. It should also be noted that it is not appropriate to categorize supersonic combustion as either constant pressure or constant volume as is sometimes helpful with subsonic combustion. For example, a gas turbine combustor and internal combustion engine can be effectively phenomenologically modeled using constant pressure and constant volume reactor models, respectively. The pressure rise in a scramjet is a result of compressibility of the working fluid and a function of its Mach number. A recent overview is provided by Urzay [73].

The rising pressure in a supersonic combustor acts as a back-pressure to the upstream supersonic inflow further slowing it down, and steepening and increasing the strength of any shock waves. The combustion-induced pressure can continue to increase until the value of the combustor pressure is about equal to that corresponding to the normal shock pressure rise of the combustor entrance flow. Any further increase in the combustor pressure will cause the flow to become "unstarted," that is, any shock wave system that formed upstream of the combustor must move further upstream and out of the inlet in order to reduce the mass flow rate through the engine to match that which the combustor pressure rise could physically support.

For nonpremixed systems, the relative velocity of the reactant streams is quantified by the velocity difference parameter, and it could be subsonic or supersonic as further quantified by the convective Mach number. Both the velocity difference parameter and the convective Mach number are relevant to the reactant mixing process and therefore combustion rate control in canonical problems [74–76]. Both quantities are important rate-controlling parameters in subsonic and supersonic combustion, but large velocity differences and supersonic convective Mach numbers are more commonly encountered in supersonic reacting flows because parallel-moving supersonic reactant streams can more readily exhibit velocity differences with values close to the speed of sound. Nevertheless, high convective Mach numbers can still be achieved for subsonic reactant streams if they are traveling in opposite directions, which is rare in practice. The primary impact of high values of the velocity difference parameter is an increased turbulence mixing rate of the mixing layer between the reactant streams. The convective Mach number has a limited competing effect in that the mixing rate could be suppressed by as much as a factor of about five as the convective Mach number increases to supersonic values [77]. The high velocity differences between the reactant streams can also induce viscous heating, which can alter the local temperature of the reactants, and therefore, reduce the ignition delay time of the local reactive mixture.

The shock waves and expansions that form in a supersonic combustor also interact with the combustion processes through the pressure and temperature changes they impart to the reactants and the generation of the baroclinic torque as they pass across the reactant mixing layer. Similar to viscous heating, the changes to pressure and temperature alter the response of the chemical kinetics, whereas the baroclinic torque introduces large-scale mixing, which increases the fuel-air interface, allowing molecular diffusion to mix the fuel and air at the molecular level where reactions take place.

Because of the strong interdependence among these various compressible flow processes and chemistry, it is hard to envision how a flamelet manifold could be generated a priori for supersonic combustion and contain all the relevant reactant states.

4 Flamelets and Supersonic Combustion

Although the utility of the flamelet model, and especially the flamelet progress variable (FPV) model, has been demonstrated extensively for numerous low speed applications, these models in their original form are unable to account for many of the physical processes characteristic of high speed reacting flows, such as variable combustion pressure, viscous heating, significant heat transfer at the walls, and varying flow properties of the reactants due to the compressibility effects, e.g., shocks and expansions. Several attempts at extending the FPV model formulation to high-speed compressible flows have been made. These attempts focus primarily on addressing the pressure dependence [78–80] of the flamelet manifold, which is the simplest and most obvious way to proceed within the framework of the existing flamelet equations.

The most common way to partially, but efficiently, account for the varying pressure in a supersonic combustor is to scale the tabulated reaction source term of the progress variable, Eq. (19), by a ratio of the square of the local mean pressure to the square of the reference pressure of the tabulated flamelet table, i.e.,

$$\overline{\dot{\omega}}_C = \frac{\overline{p}^2}{p_{ft}^2} \overline{\dot{\omega}}_{C_{ft}}, \tag{20}$$

where the subscript ft denotes the quantity obtained from the flamelet table. The pressure scaling of the progress variable reaction rate is motivated by the fact that the majority of chemical reactions are second order. However, although this scaling offers a physically reasonable approximate way to relate reaction rates at two different combustion pressures, it does not account for the differences in the equilibrium flame temperature or changes to the mixture composition, and therefore mixture fraction and progress variable, that also occur when the finite rate kinetics are actually evaluated at different pressures. Nevertheless, this approach has been demonstrated to improve the pressure predictions of HyShot II experiments [81].

More recently, to improve the accuracy of the pressure scaling of the progress variable reaction source term with respect to a generic chemical kinetics mechanism, Saghafian et al. [80] introduced a generalized scaling that includes a density power scaling and an activation temperature scaling in the form:

$$\overline{\omega}_C = \left(\frac{\overline{\rho}}{\rho_{ft}}\right)^{a_p} \exp\left(-T_a\left(\frac{1}{\widehat{T}} - \frac{1}{T_{ft}}\right)\right)\overline{\omega}_{C_{ft}}, \qquad (21)$$

where a_p and T_a are scaling constants that can be optimized a priori to improve the pressure scaling method over the range of pressures of interest. In practical applications, reasonable values for a_p and T_a range from 2–3, and 10,000–20,000, respectively.

While the scaling approach is certainly a way to introduce some influence of the variable pressure via a progress variable source term, the most direct way to account for the varying pressure within a flamelet framework is simply to add the pressure as a parameterizing variable to the flamelet table. This approach increases the computer memory footprint of the flamelet table by as much as an order of magnitude and further increases the computational cost of lookup and retrieval; however, it eliminates the approximations associated with the pressure scaling approach and significantly improves the robustness of the progress variable in supersonic combustion applications such that some regularization procedures proposed by [27] may not be needed, as demonstrated by Quinlan [82].

5 HIFiRE Direct Connect Rig (HDCR)

To demonstrate some of the challenges of utilizing flamelet models for supersonic combustion applications, RAS of the HDCR combustor are performed for two flight conditions corresponding to flight Mach numbers of 5.84 and 8. The first condition is referred to as the dual-mode case and exhibits regions of both subsonic and supersonic combustion. The second condition corresponds to the scram-mode and exhibits primarily supersonic combustion, albeit in both nonpremixed and premixed combustion modes. The two flight conditions cover a range of combustion phenomena that could be reasonably expected to commonly occur in a scramjet engine during flight.

The HDCR was a ground-based direct-connect experiment conducted at NASA Langley Research Center (LaRC) in support of the HIFiRE 2 flight experiment [37, 39]. HIFiRE 2 was a hydrocarbon-fueled scramjet flowpath designed to demonstrate supersonic-combustion mode transition from dual-mode to scram-mode operation and to validate design and analysis tools. Based on the estimated flight trajectory, supersonic combustion mode transition was expected to occur between flight Mach numbers of about 6–8. The HDCR ground experiment was developed and performed prior to flight of the HIFiRE 2 article to validate the flowpath design and demonstrate combustor operability in the range of flight Mach numbers from 6 to 8.

The HDCR ground test article included the constant-area isolator, cavity-based combustor with multistage fuel injection, and a bifurcated exhaust nozzle. An inner mold line of the flowpath is shown in Fig. 1, in which relevant dimensions and injector locations are indicated. The HIFiRE 2 inlet was not included in the HDCR test article, instead, the HDCR isolator was connected directly to the ground test facility CD nozzle. The flow properties, including the Mach number, at the entrance of the isolator were obtained from two CFD simulations [83] of the HIFiRE 2 inlet at flight Mach numbers of 5.84 and 8. These inlet simulation results showed that the facility nozzles, with Mach numbers of 2.51 and 3.46, produced isolator flows appropriate for the dual-mode and scram-mode experiments, respectively. The total enthalpy of each of the two flows was set to match that of the corresponding flight Mach number. The HDCR combustor has five stages of fuel injectors; however, only the primary and secondary injectors located upstream and downstream of the cavity, respectively, were fueled during the experiments. In the HDCR experiments, dual-mode operation was marked by the leading combustion-induced shock anchoring upstream of the primary injectors. When this leading shock moved downstream of the primary injectors, the flowpath was operating in scram-mode. The fuel used was a JP-7 surrogate consisting of a gaseous mixture of 36% methane and 64% ethylene by volume [84]. The dual-mode and scram-mode cases were tested with a total equivalence ratio of 0.65, and 1.0, respectively. The total equivalence ratio was further split between the primary and secondary injectors, with values of 0.15 and 0.5 for the dual-mode case and 0.4 and 0.6 for the scram-mode case, respectively. These fuel splits were set to demonstrate on the ground one of the primary objectives of the HIFiRE 2 flight experiment, which was to reach combustion performance of burned equivalence ratio of 0.7 at Mach 8 [37]. Hereafter, simulation cases will be referenced using a case identifier that reflects the operational mode, the flight Mach number, and the imposed simulation wall boundary conditions, as shown in Table 2. For example, case *D584A* signifies dual-mode operation, *D*, at a flight Mach number of *5.84* with adiabatic walls, *A*. Similarly, case *S800I* signifies scram-mode operation, *S*, at a flight Mach number of *8.00* with isothermal walls, *I*. Data collected during the experiments included wall temperatures, heat fluxes, and wall static pressures. The flowpath was outfitted with 144 static pressure ports, 19 flowpath surface thermocouples, and 4 heat flux gauges.
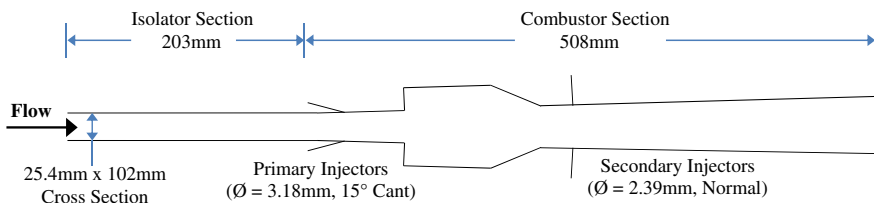

Fig. 1 Side view and key dimensions of the HDCR combustor flowpath, where $\oslash$ is internal diameter of the injectors

Table 2 Summary of simulated test cases, including flight Mach number, plenum total conditions, fuel equivalence ratios (Φ), and wall boundary conditions (BCs)

Case	Flt. mach	Tot. temp. (K)	Tot. pres. (atm)	Pri. inj. Φ	Sec. inj. Φ	Wall BC
D584A	5.84	1550	14.63	0.15	0.5	Adiabatic
D584I	5.84	1550	14.63	0.15	0.5	Isothermal
S800A	8.00	2570	42.19	0.40	0.6	Adiabatic
S800I	8.00	2570	42.19	0.40	0.6	Isothermal
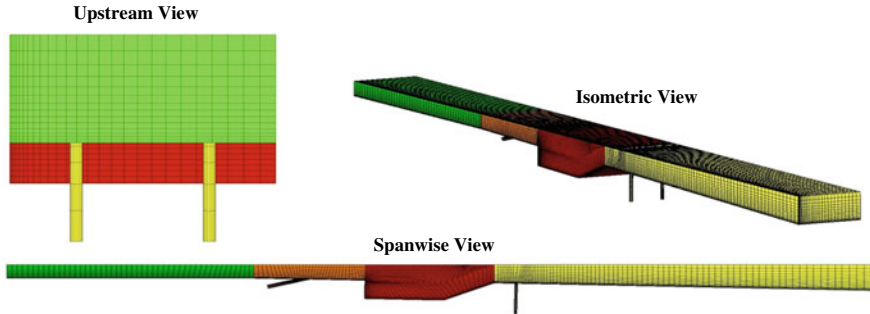
Fig. 2 Looking upstream, isometric, and side views of the structured, quarter-geometry, grid used for RAS of the HDCR combustor coarsened four times for visual clarity

5.1 Numerical Approach

To simulate the HDCR experiments, the Favré-averaged RAS equations were solved using VULCAN-CFD. VULCAN-CFD is a structured-grid finite-volume solver that is extensively used for high-speed combustion simulations using RAS techniques [85]. For the current study, a 6.6 million cell, quarter-geometry, structured grid was used, which is illustrated in Fig. 2. This grid included the facility nozzle, which is not shown. Wall spacing was set for the application of wall-matching functions [86] with y+ values not exceeding approximately 30. Symmetry was enforced at the appropriate boundaries, and an extrapolation of transported variables was applied at the outflow plane. Simulations were also performed using adiabatic and isothermal wall boundary conditions to determine the effect of wall heat losses. In the case of isothermal walls, a one-dimensional heat-conduction equation was solved for the heat transfer through solid surfaces given the wall external temperature and thermal conductivity, which were set to yield wall temperatures similar to those measured during the experiment [87]. The governing RAS equations were closed using the blended k-ω/k-ϵ turbulence model of Menter [88]. Inviscid fluxes were calculated using the low-dissipation flux-split scheme (LDFSS) of Edwards [89]. The van Leer

flux limiter was used, along with a monotone upstream-centered scheme for conservation laws (MUSCL) with an interpolation coefficient (κ) of 1/3. The equations were integrated in pseudotime using an implicit diagonalized approximate factorization (DAF) scheme [90] with a maximum local CFL number of 2.0.

Reaction chemistry was modeled using an 18-step reduced chemical reaction mechanism designed for the combustion of ethylene [38]. Transport equations for the 22 species comprising the reaction mechanism were solved implicitly, and no TCI model was used (aka laminar chemistry assumption). The turbulent Prandtl number was set to 0.89 for each case, and the turbulent Schmidt number was set to 0.325 for the dual-mode case and 0.25 for the scram-mode case, as suggested by Storch et al. [37]. Laminar Prandtl and Schmidt numbers were set to 0.72 and 0.22, respectively [37].

It should also be noted that no transport equation for the mixture fraction, mixture fraction variance or the progress variable were solved in the current work. Instead, these quantities were computed from the RAS data during the postprocessing and analysis step.

5.2   Simulations of the HDCR

Figures 3 and 4 show wall pressure vs. axial distance for simulations and the experiment for dual-mode (D584A and D584I) and scram-mode (S800A and S800I) cases, respectively. All simulations predict the general trends and values of the centerline experimental wall static pressure data. The pressure is slightly overpredicted throughout the isolator for the dual-mode cases and almost 20% for the scram-mode cases. This greater overprediction is due to the thermodynamic nonequilibrium effects [91], which were not modeled in the current simulations. Nevertheless, all simulations still captured the location of the leading oblique shock due to combustor pressure rise but overpredict somewhat the combustor and combustor peak pressures. The isothermal scram-mode case, S800I, overpredicts the combustor peak pressure the most. The differences in the isothermal and adiabatic solutions are a direct indication of the sensitivity of the flowfield to wall heat transfer, which increases for the scram-mode case because of the higher total temperature. Despite some of the noted discrepancies between the simulations and experiments, this qualitative level of agreement is likely sufficient for current analysis of the flamelet modeling assumptions.

Figures 5 and 6 show the contours of the Mach number in the spanwise center plane and through the middle of the injector centerline for the dual-mode and scram-mode cases, respectively. The black lines denote an isocontour of the sonic line. The leading shock due to combustor pressure rise resides upstream and downstream of the primary injectors for the dual- and scram-mode cases, respectively. The leading oblique shock serves to stabilize flames that anchor near the primary injector ports. The flow subsequently separates at the rearward-facing step corner, and a shear layer forms over the recirculating flow within the cavity. This shear layer reattaches near the point of cavity closeout. The mixture of air, partially reacted fuel from the primary
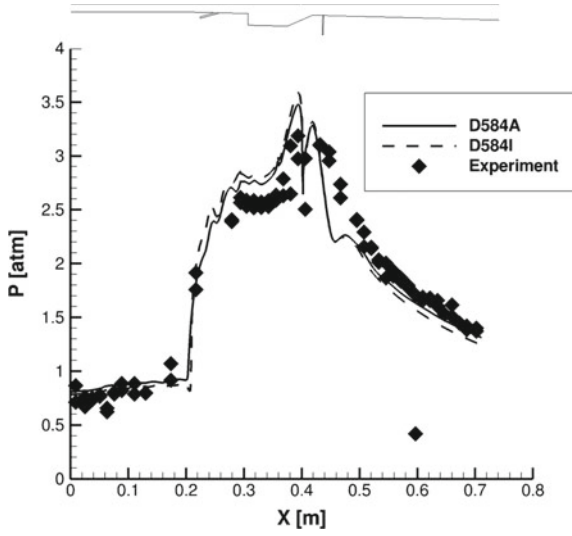
Fig. 3 Comparisons of streamwise (x) wall static pressure (p) data obtained from simulations D584A and D584I and experimentally for dual-mode operation of the HDCR combustor
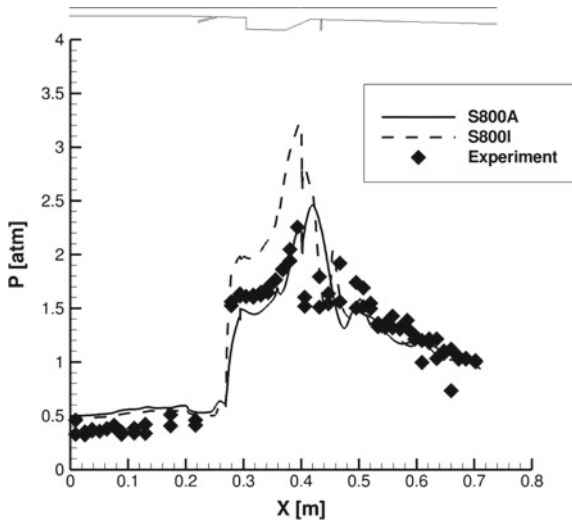

Fig. 4 Comparisons of streamwise (x) wall static pressure (p) data obtained from simulations S800A and S800I and experimentally for scram-mode operation of the HDCR combustor
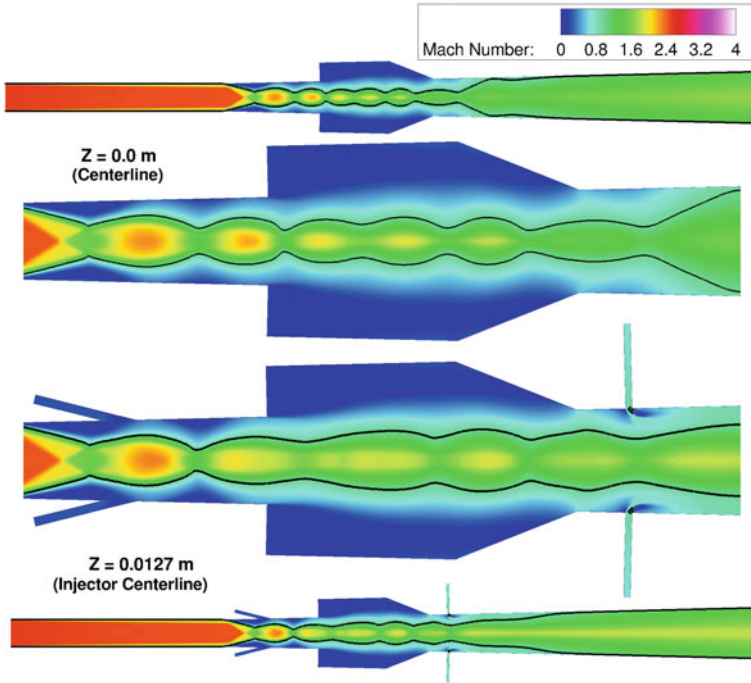
Fig. 5 Contours of the Mach number at spanwise (z) center plane and middle injector centerline for case D584A. Dark black lines correspond to the sonic isocontour

injectors, and some combustion products convect downstream where it further mixes with fresh fuel injected by the secondary injectors.

Because the majority of fuel for both flight conditions is delivered through the secondary injectors, the distribution of the heat release is shifted toward the secondary injectors. The normalized chemical heat release is shown in Figs. 7 and 8. For the dual-mode cases, the peak heat release occurs within the subsonic portions of the flowfield, whereas for the scram-mode cases, the combustion occurs predominantly at supersonic flow velocities. Of further note are the differences in flame location and structure. In the dual-mode case, the flame anchors directly outside of the primary injector ports, whereas in the scram-mode case, the primary injector fuel burns downstream of the injectors in a more distributed fashion. The flames anchored at the primary injection site reside behind the leading oblique shock and above the cavity region. The flames forming at the secondary injector site, for dual- and scram-mode cases, appear to be of a similar nature.
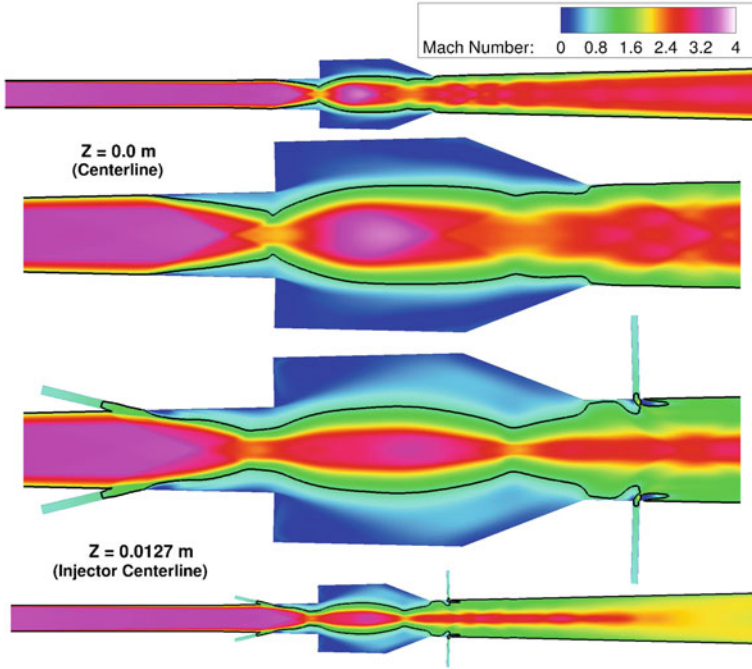
Fig. 6 Contours of the Mach number at spanwise (z) center plane and middle injector centerline for case S800A. Dark black lines correspond to the sonic isocontour

6   Combustion Mode Analysis for the HDCR

Assessing the applicability of flamelet models for a turbulent reacting flow requires one to consider the extent to which the flowfield meets the fundamental flamelet model assumptions. In the case of nonpremixed combustion, for which the flamelet resides near the surface of stoichiometric mixture fraction, and for which the scalar dissipation rate couples the flame dynamics to that of the fluid dynamics, the characteristic chemical time scale must be considerably smaller than that of the representative diffusive and turbulent transport processes. This means that the Damköhler number (Da), which is the ratio of a characteristic flow time scale, τ_{flow}, to that of chemistry, τ_{chem}, must be much greater than unity, indicating that the characteristic reaction chemistry times are much shorter than those of the characteristic flow processes.

In the case of premixed combustion, for which the flame can propagate normal to itself, the chemical time scale and thermal diffusivity effectively govern the flame thickness, which must be considerably smaller than the representative turbulent length scales under the flamelet assumption. This means that the Karlovitz number (Ka) defined as the ratio of a characteristic flame length scale to a characteristic tur-
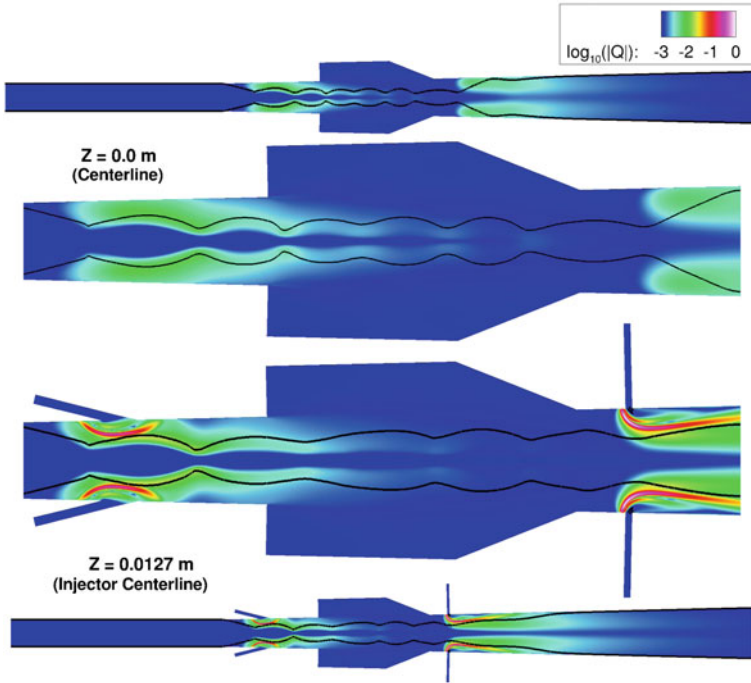
Fig. 7 Contours of the logarithm of chemical heat release (Q) normalized by its global maximum for simulation D584A. Dark black lines correspond to the sonic isocontour

bulence length scale, must be much less than unity. In most cases, the Kolmogorov scale is used as the representative turbulence length scale.

In the current work, the Favré-averaged RAS solutions for HDCR cases D584A and S800A are used to determine when the fundamental flamelet model assumptions are satisfied and/or violated for a scramjet combustor. To accomplish this, a flame index is first devised to identify regions of chemical activity. Once those regions are identified, a flame-weighted Takeno index is computed to identify regions of premixed and nonpremixed combustion. Local Da is subsequently estimated using the approach outlined by Poinsot and Veynante [2] and Peters [13]. Proxy combustion diagrams are devised for the nonpremixed combustion using the flame-weighted Takeno index and Da. Finally, a priori investigation of the effects of pressure and compressibility, wall heat transfer, and flamelet boundary condition variability on the HDCR flames is presented.
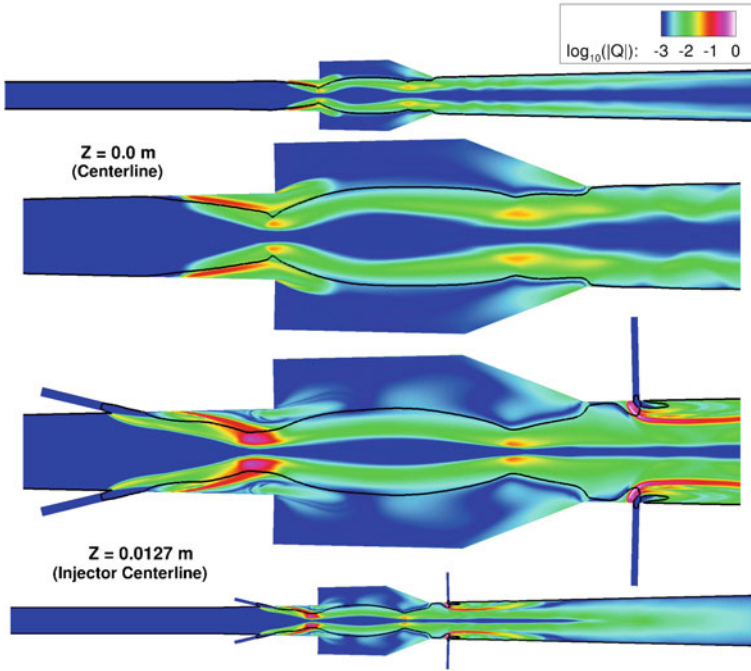
Fig. 8 Contours of the logarithm of chemical heat release (Q) normalized by its global maximum for simulation S800A. Dark black lines correspond to the sonic isocontour

6.1 Flame Index

The first step in characterizing the combustion fields is to devise a metric indicative of flame activity, which can be used to identify regions of combustion. The current study uses the approach of Lacaze et al. [92] and defines a flame index, f,

$$f(x, y, z) = \frac{\max_{\alpha}(\bar{\dot{\omega}}_{\alpha}(x, y, z))}{\max_{(x,y,z)}(|\bar{\dot{\omega}}_{\alpha}|)}, \tag{22}$$

where $\bar{\dot{\omega}}_{\alpha}$ is the Favré-averaged production rate of species α and x, y, and z are Cartesian coordinates. The subscript attached to the max operator indicates what quantity the max operation is applied to. The flame index is defined such that it indicates the level of maximum chemical production over all species in the finite-rate reaction mechanism used in the simulations. The index takes on a value between 0 and 1, where 0 corresponds to no chemical production and where 1 corresponds to a point at which at least one chemical species is produced at its global maximum.

Contours of $\log_{10}(f)$ for cases D584A and S800A are presented in Figs. 9 and 10, respectively. The flame index indicates that for dual-mode operation, case D584A,
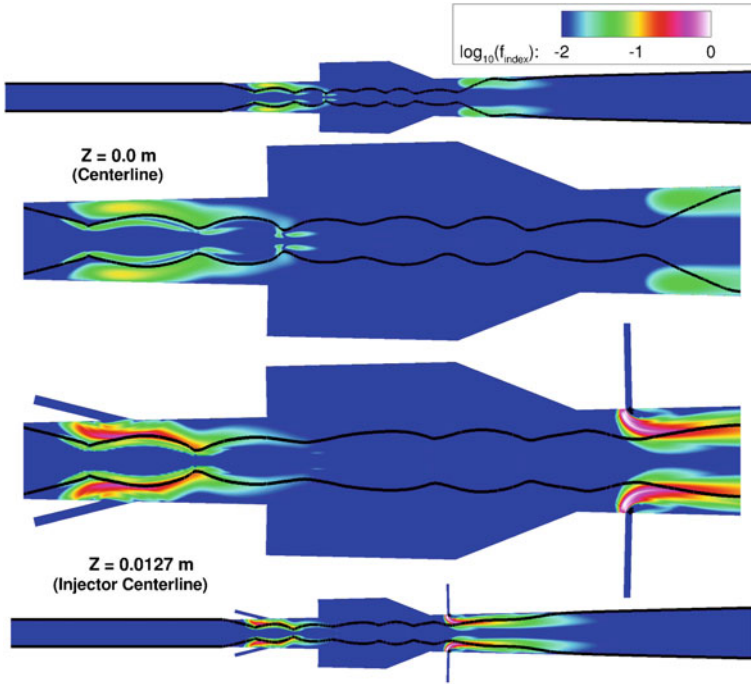
Fig. 9 Contours of the logarithm of flame index, f, for simulation D584A. Dark black lines correspond to the sonic isocontour

thin flames anchor near the primary injector orifices, which are stabilized by the leading oblique shock and recirculating fluid directly outside the injectors. Thin flames also burn outside the secondary injector orifices and extend downstream. For case S800A, the flames associated with the primary injectors appear to be fundamentally different than those of the secondary injectors. Although there does exist a thin region of combustion near the injectors stabilized by the fuel injection bow shock and fluid recirculation, most of the combustion appears to be distributed from the point of injection to just downstream of the cavity step corner. When compared to the Mach number contours in Fig. 6, the combustion appears to correlate with the leading shock until a pronounced increase in flame intensity is seen directly behind the point of the leading shock-shock interaction. This observation may suggest the occurrence of shock-induced combustion. Downstream of this intense region of combustion, a weak distributed flame is observed. However, it should be noted that some of the differences in the flame topology could be attributed to the difference in equivalence ratio at the primary injectors for the dual- and scram-mode cases. The secondary injector flames for the scram-mode are similar in nature to those observed in the dual-mode cases, which suggests a relatively thin flame that extends downstream past the injectors and is angled toward the wall.
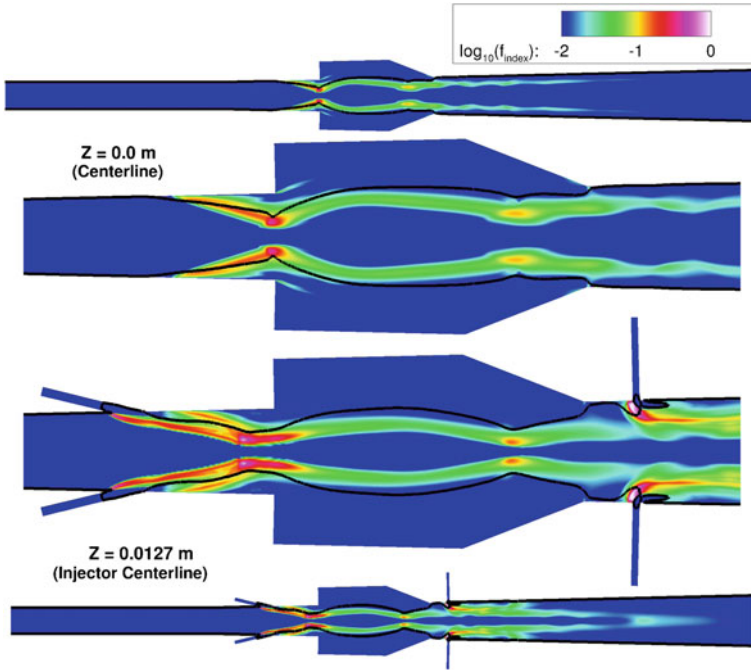
Fig. 10 Contours of the logarithm of flame index, f, for simulation S800A. Dark black lines correspond to the sonic isocontour

6.2 Combustion Mode

To isolate the nonpremixed combustion data from that of the premixed data, the approach of Yamashita et al. [93] is used. This method assumes that in nonpremixed flames, the gradients of oxidizer and fuel species are oriented in opposite directions, while in premixed flames, the gradients are oriented in the same direction. By taking the dot product of the gradients and normalizing, the Takeno index, Λ_T, can be obtained:

$$\Lambda_T = \frac{\nabla \widetilde{Y}_{oxidizer} \cdot \nabla \widetilde{Y}_{fuel}}{|\nabla \widetilde{Y}_{oxidizer} \cdot \nabla \widetilde{Y}_{fuel}|}, \qquad (23)$$

where $\widetilde{Y}_{oxidizer}$ and $\widetilde{Y}_{fuel}$ are the Favré-averaged oxidizer and fuel species mass fractions, respectively. For the current work, the Takeno index is obtained using the oxidizer (O_2) and fuel (CH_4, C_2H_4) mass fractions. When the gradients of these mass fractions are aligned, the index returns 1.0, which indicates premixed combustion. Whereas, when these gradients are of opposite sign, the index returns -1.0, which indicates nonpremixed combustion. In the context of RAS, the Takeno index indicates the statistically-dominant combustion mode at a given location in the flowfield. Since the RAS solution is an averaged representation of the flowfield, either premixed

or nonpremixed regions of the RAS flowfield may in actuality exhibit periods of nonpremixed or premixed combustion. The effect of such intermittency can only be captured using LES or DNS.

By further weighting the Takeno index by the flame index, a new index, flame-weighted Takeno index, Λ_f, is formed:

$$\Lambda_f = f \Lambda_T \tag{24}$$

The value of Λ_f ranges from $-1.0 < \Lambda_f < 1.0$ and conveys both the flame intensity and dominant combustion mode at each point in the flowfield. Accordingly, Λ_f is used in subsequent analysis to identify the combustion character of the HDCR.

Additionally, the Da is also computed for both nonpremixed and premixed combustion. The Da is the ratio of a characteristic flow time scale, τ_{flow}, to that of the chemistry, τ_{chem}. When Da is large, there exists a separation of chemistry and flow scales such that the fundamental assumption of a flamelet model, i.e., that a thin laminar flame is only distorted by a background turbulent flowfield, is satisfied. However, when Da approaches unity, the flamelet assumptions break down as the turbulence and chemistry begin to interact and interfere with one another.

To compute the Da for nonpremixed combustion, the characteristic flow time scale is approximated using the scalar dissipation rate, χ (Eq. 18), which has the units of inverse time. The scalar dissipation rate is modeled using the approach of Poinsot and Veynante [2],

$$\chi_{modeled} = C_a \frac{\epsilon}{k} \widetilde{Z''^2}, \tag{25}$$

where ϵ, k, and C_a are the turbulence dissipation rate, turbulence kinetic energy, and a model constant set to unity [2]. When the mixture fraction variance is not available, its upper limit can still be computed, $\widetilde{Z''^2}_{max} = \widetilde{Z}(1 - \widetilde{Z})$, by using the boundedness property of the mixture fraction. This is useful when considering the limiting values of the Da. That is, using the maximum value of the mixture fraction variance to model the scalar dissipation rate and flow time scale lowers the value of the Da, which implies a conservative view of the applicability of the flamelet model. To estimate the characteristic time scale of the chemistry, a mass fraction and production rate of water are used,

$$\tau_{chem} = \frac{\bar{\rho}\widetilde{Y}_{H_2O}}{\bar{\dot{\omega}}_{H_2O}} \tag{26}$$

The Da is then computed as,

$$Da_{nonpremixed} = \frac{1}{\chi_{modeled}\tau_{chem}}. \tag{27}$$

For the case of premixed combustion, the Da is typically defined as the ratio of characteristic turbulence and flame time scales,

$$Da_{premixed} = \frac{\tau_{turb}}{\tau_{flame}} = \frac{l/u'}{l_F/s_L}, \tag{28}$$

where l_F, s_L, l, and u' are the laminar flame thickness and speed, integral turbulence length, and turbulence fluctuating velocity, respectively. However, the most appropriate turbulence scale for calculating the Da for premixed flames is unclear [2]. In the current work, the premixed Da is calculated using the integral turbulence length scale. The laminar flame thickness and laminar flame speed are estimated by solving freely-propagating premixed flames corresponding to the average temperature, pressure, and fuel equivalence ratio characterizing the premixed data within the flowfield, as identified by the flame-weighted Takeno index.

Scatter plots of the logarithm of the Da versus the flame-weighted Takeno index for the primary and secondary injector flames for case D584A are shown in Fig. 11. The same plots for case S800A are shown in Fig. 12. In each figure, the nonpremixed Da is used for data corresponding to $\Lambda_f < 0$, and the premixed Da is used for $\Lambda_f > 0$. The data points are sized by the chemical heat release rate and are colored by the production rate of water. Each figure includes only the data contained within the gray regions on the included flowpath diagram. These regions focus the analysis on the primary and secondary injection. The data within $0.03 < \Lambda_f < 0.03$ are omitted for clarity.

For case D584A, Fig. 11 suggests that, for both the primary and secondary injector flames, the combustion occurs primarily at high Das ($Da >> 1$) and in a non-premixed mode ($\Lambda_f < 0$). Although limited regions of premixed combustion exist for this case, the heat release associated with those regions is small as compared to that of the nonpremixed combustion. These figures suggest that for case D584A, the fundamental assumptions made for nonpremixed flamelet models are likely satisfied and that such models may sufficiently predict the combustion physics governing dual-mode operation of the HDCR flowpath.

For case S800A, Fig. 12 suggests that the combustion is of a more complex nature. For the primary injectors, the combustion occurs over a range of Das and is split among both nonpremixed and premixed modes. A significant portion of the heat release due to the primary injectors corresponds to premixed regions of combustion occurring near $Da = 1$, suggesting that the characteristic flame time scale is on the same order of magnitude as that of the integral turbulence. However, a significant portion of the nonpremixed combustion occurs at high Da numbers as well. For the secondary injectors, the combustion occurs at a range of Das and primarily in a nonpremixed mode. Based on these data, a suitable simulation of the HDCR flowpath for scram-mode operation would likely require both premixed and nonpremixed flamelet models, and the fundamental assumptions made for these models may only be valid for limited regions of the combustion.

Fig. 11 Log of the Da, versus flame-weighted Takeno index, Λ_f, for case D584A. Data points are sized by chemical heat release, $\widetilde{Q}$, and colored by normalized production rate of water, $\bar{\omega}_{H_2O}$. Data are plotted for the primary injector (top) and secondary injector (bottom) portion of the flowpath as denoted by the gray regions on the included flowpath diagrams
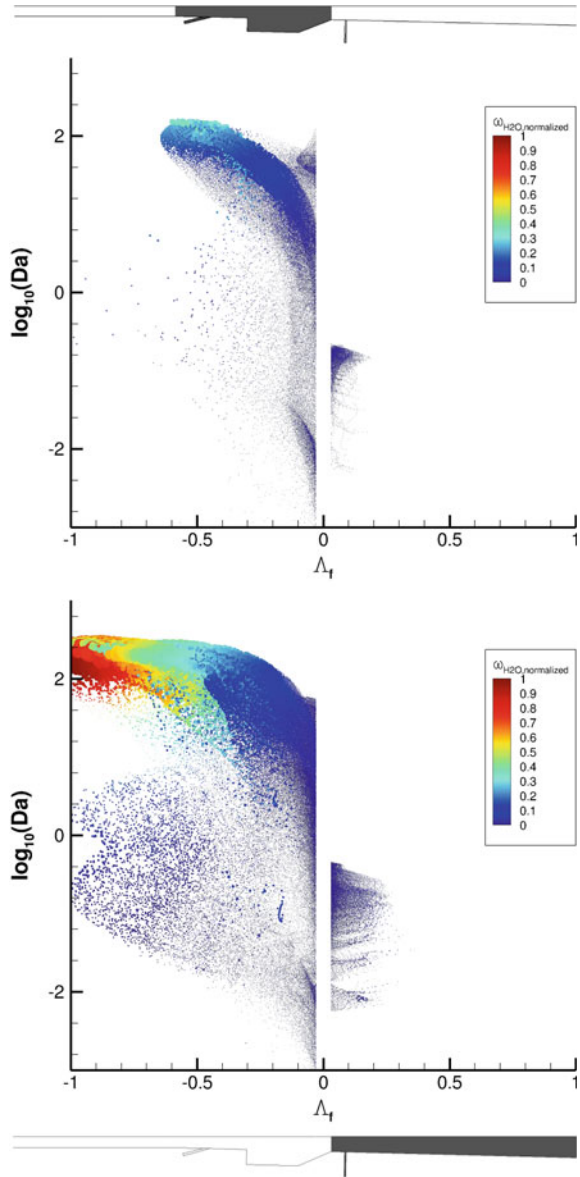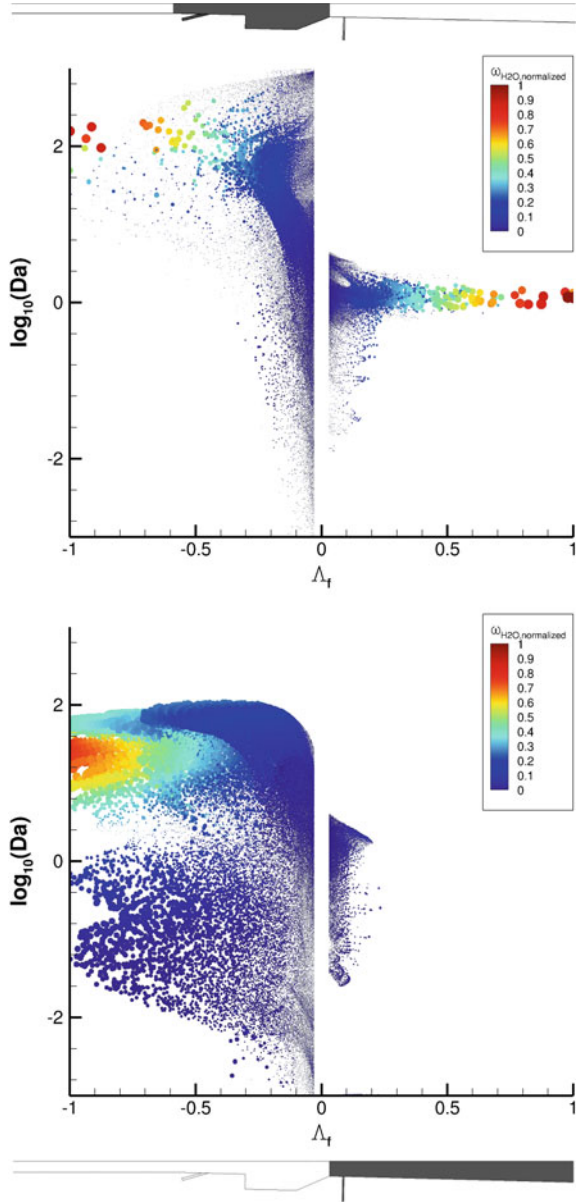
Fig. 12 Log of the Da, versus flame-weighted Takeno index, Λ_f, for case S800A. Data are sized by chemical heat release, $\tilde{Q}$, and colored by normalized production rate of water, $\bar{\dot{\omega}}_{H_2O}$. Data are plotted for the primary injector (top) and secondary injector (bottom) portion of the flowpath as denoted by the gray regions on the included flowpath diagrams

7 Effect of the Pressure

Figure 13 shows scatter plots of the mean static temperature vs. the Favré-averaged mixture fraction for cases D584A and S800A for both the primary and secondary injection regions. Since the majority of the combustion occurs in a nonpremixed mode, the mixture fraction provides a convenient parameterization of the three-dimensional flowfield data for visualizing the influence of the pressure on combustion. The scatter data are colored by the logarithm of the mean static pressure, which allows for identifying regions of significant variations in pressure. The variation in pressure appears to be generally higher for case S800A, although case D584A exhibits significant variation as well. The scram-mode data appear to span approx-
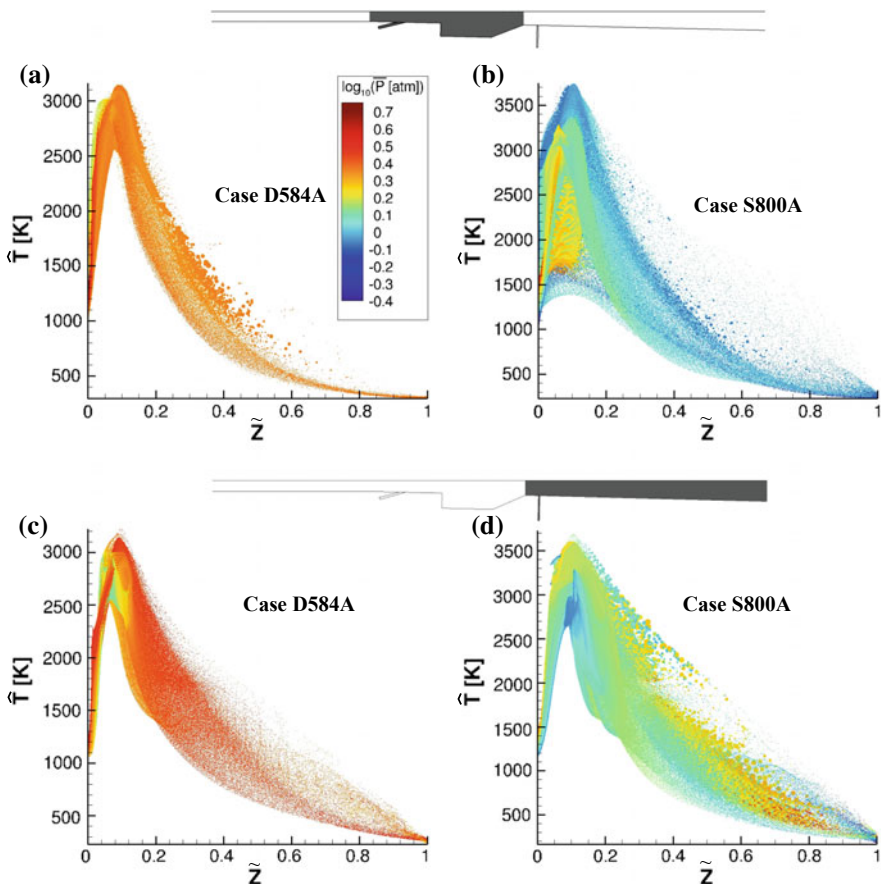

Fig. 13 Static temperature, $\widehat{T}$, versus mixture fraction, $\widetilde{Z}$, colored by the logarithm of static pressure, $\bar{P}$, and sized by chemical heat release rate, $\widetilde{Q}$, for **a** case D584A and **b** case S800A, primary injector flames and for **c** case D584A and **d** case S800A, secondary injector flames

imately half an order more of static pressure as compared to the dual-mode data, for which the static pressure spans nearly an entire order of magnitude. In addition, these pressure variations occur near stoichiometry, which is where the majority of heat is released as well. Thus, these observations indicate that any suitable flamelet model must account for pressure variations due to combustion and compressibility for application to a dual-mode scramjet combustor.

8   Effect of the Wall Heat Transfer

In addition to pressure variations and compressibility effects, recent efforts in developing flamelet models have been directed at including the effects of heat transfer. As with pressure, the focus has been on developing modifications to existing incompressible flamelet models to account for wall heat losses using various approaches [94–97]. In this section, the effect of heat loss on the flame structure is illustrated by analyzing the simulations computed with and without wall heat transfer. The primary mechanism by which wall heat transfer influences the combustion field is local quenching in the vicinity of the wall. For scramjet engines, in which the core flow is at high velocity and fuel is injected through the walls, a considerable amount of fuel is entrained in the slow-moving near-wall regions. As a result, the fuel has sufficient time to mix with oxidizer and react, thereby creating intense regions of combustion near the wall surfaces. Figure 14 shows scatter plots of the mean static temperature vs. the Favré-averaged mixture fraction for cases D584A and S800A (adiabatic), and D584I and S800I (isothermal) for the entire combustor section. The scatter data are colored by the logarithm of the velocity magnitude, V_s, which allows for identifying the near-wall regions denoted in dark blue. By examining the minimum velocity magnitude data, near-wall flame quenching by heat loss through the wall can be directly observed for the isothermal cases D584I and S800I. Nevertheless, these data show that relatively low temperature combustion is still taking place in the near-wall regions. For the adiabatic cases, D584A and S800A, the near-wall data exhibit high temperature, near-equilibrium values, which indicates fully burning flames. While these differences are striking and may suggest the requirement for inclusion of a heat loss model in a general compressible flamelet model, for the HDCR, the adiabatic simulations yielded more accurate solutions when compared to experimental static pressure data, suggesting that either the isothermal simulations significantly overpredicted the heat transfer, or the aggregate effect of wall heat transfer on the combustion and heat release is limited.
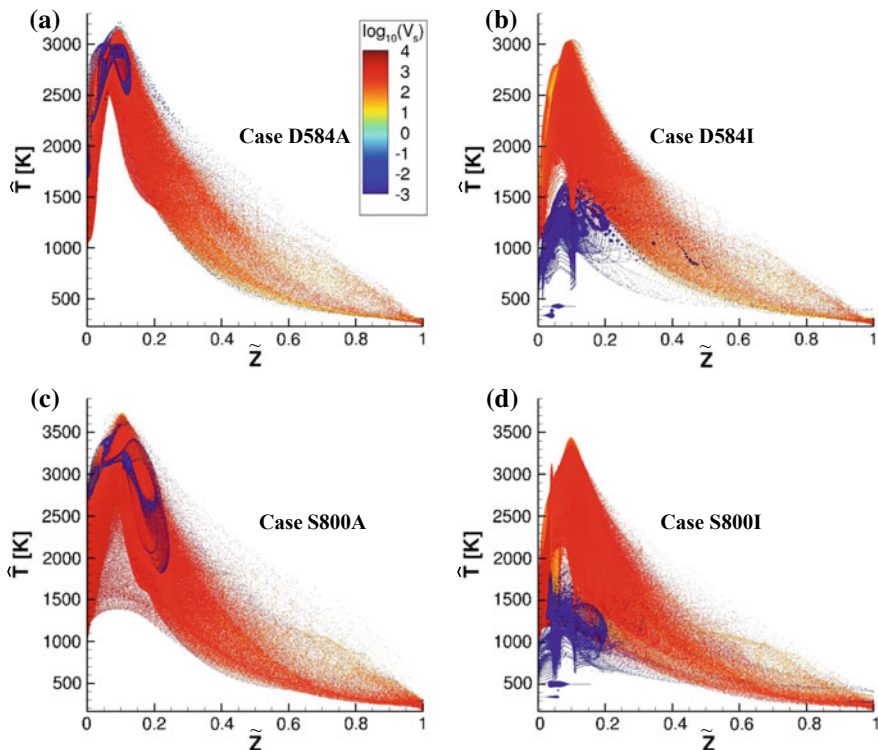
Fig. 14 Static temperature plotted in mixture fraction space and colored by logarithm of velocity magnitude, V_s, for cases **a** D584A, **b** D584I, **c** S800A, and **d** S800I, showing the effect of heat losses on the combustion

9 Effect of the Flamelet Model Boundary Conditions

The effect of the flamelet model boundary conditions is probably the least investigated and addressed issue facing flamelet models for compressible turbulent reacting flows. This is because the process of specifying applicable ranges for fuel and oxidizer temperatures and pressures a priori for flamelet equations is unclear. For example, since for supersonic flow pressure varies with flowpath geometry and across shocks and expansion waves, determining the appropriate pressures at which flames mix and react to build a flamelet table for a scramjet combustor is impossible without prior knowledge of the heat release rate and the flowfield. In this regard, a compressible flamelet model is fundamentally different from conventional incompressible flamelet models used in applications where the combustor pressure can typically be assumed to be approximately constant and known a priori, and where the pure fuel and oxidizer temperatures remain at their known injected values.

To obtain the information about the flamelet equation boundary conditions appropriate to a specific compressible flow, in general, one must perform a turbulent react-
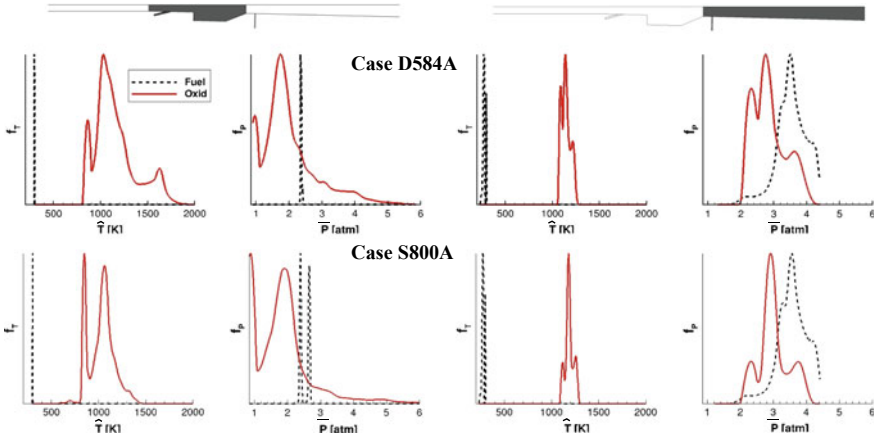
Fig. 15 PDFs of static temperature and pressure (f_T and f_P, respectively) for fuel ($Z > 0.99$) and oxidizer ($Z < 0.01$) conditions for cases D584A (top) and S800A (bottom). Regions from which the data are sampled are shown above the respective plots, with the leftmost representing the primary injector flames and the rightmost representing the secondary injector flames

ing flow simulation that does not utilize a flamelet model. After performing such a simulation, the simulation data must be analyzed and, at a minimum, fuel and oxidizer temperatures and pressures must be extracted for regions of the flowfield where a flame index indicates the presence of combustion. With this data, one may then construct PDFs to determine the range and the likelihood of specific flamelet boundary conditions required to model the combustion, and potentially use this information to select a most likely set of boundary conditions. The flamelet table is subsequently built by solving the flamelet equations for these conditions. Alternately, flamelet tables may be built for a range of boundary conditions as long as a unique parameterization for them can be developed. One such attempt is discussed by Quinlan [82]. Furthermore, for the case of multiple injectors, it is also prudent to tailor the analysis to each injector set independently and to determine whether a multiple mixture fraction approach may be appropriate [98, 99].

To estimate the range and likelihood of different flamelet equation boundary conditions in the HDCR combustor, all mixture fraction data less than 0.01 and greater than 0.99, for pure oxidizer and pure fuel, respectively, were isolated from the solution. These data were then split into two groups according to whether the data resided in the primary or secondary injector regions. PDFs were then constructed for pressure and temperature and are shown for cases D584A and S800A in Fig. 15. For both dual-mode and scram-mode operation, the fuel temperatures (dashed lines) remain about constant at their nominal values, while the oxidizer temperatures vary considerably and exhibit multimodal distributions. For the primary injectors, the fuel pressures are distributed tightly around their nominal values for the dual-mode case, whereas they exhibit some narrow-range bimodality for the scram-mode case. The oxidizer pressures exhibit broad multimodal distributions in all cases. For the sec-

ondary injectors, both the fuel and oxidizer pressures show multimodal distributions. However, these observations are not general and depend on whether the injected fuel flow is overexpanded, underexpanded or pressure matched. The observed pressure and temperature variations would be minimal for pressure matched conditions and much smaller for underexpanded than overexpanded flow conditions. This is because the flow contains only expansion waves for the fuel plumes undergoing underexpansion, whereas the same plumes contain internal shock waves during overexpansion. Therefore, because the fuel flumes are underexpanded, the fuel PDFs are narrow. On the other hand, because the oxidizer flow is always overexpanded, when the combustor provides sufficient back pressure, the oxidizer PDFs are broad.

10   Summary and Conclusions

Flamelet models have proven useful in enabling fast and accurate simulations of subsonic combustion because they can parameterize complex chemical state-space with as few as one scalar quantity, such as the mixture fraction. However, in supersonic combustion these models face many challenges. The current work presents an analysis of the steady flamelet model assumptions in supersonic combustion application. The HDCR [36, 37] dual-mode scramjet combustor is used for this purpose. Although designed for academic and collaborative purposes, the HDCR is representative of a practical cavity-stabilized scramjet combustor. The analysis uses 3D RAS data obtained using a finite-rate reaction mechanism at Mach 5.84 dual-mode and Mach 8 scram-mode flight conditions. Quantities, such as the mixture fraction and progress variable, typically used for parameterizing the flamelet models, are obtained from the RAS data in the postprocessing and analysis step. This analysis reveals that, for the HDCR, both nonpremixed and premixed combustion can be observed. Furthermore, although the majority of heat is released via nonpremixed, near-equilibrium combustion, for the Mach 8 scram-mode conditions, some heat enters the combustor via premixed combustion that includes significant finite-rate effects. These observations suggest that a multicombustion-mode flamelet model might be required to accurately simulate the Mach 8 flight conditions. Furthermore, to capture the finite-rate effects, a reaction progress variable is required in addition to the mixture fraction.

The effects of variable pressure, wall heat transfer, and flamelet equation boundary conditions were also evaluated. These three elements present key barriers to utilizing flamelets for supersonic combustion simulations. In the HDCR, the combustor pressure increases by about a factor of five. This rise is due to close coupling of thermodynamics with fluid mechanics that occurs at supersonic speeds, and occurs in the regions of the highest heat release. Several methods of accounting for rising pressure in flamelet models were discussed. The simplest is that of pressure scaling of the progress variable reaction source terms. This approach, however, neglects the pressure-induced differences in chemical composition and the adiabatic flame temperature. To account for these effects, pressure must be included as an additional parameterizing variable in the flamelet formulation.

The heat transfer to the walls can be significant at hypersonic speeds. For example, the total temperature for the HDCR ranges from about 1500–2500 K across the flight Mach number range, which would necessitate active cooling of the combustor for times longer than those for which this uncooled article was designed for. The heat transfer at the walls occurs because of two separate effects: due to slowing down and viscous heating of the flow in the boundary layers, and due to flame-wall interactions and convection of combustion products toward the wall. In the former, typically the oxidizer is cooled by the wall, thereby decreasing its enthalpy. In the latter, reacting fuel-oxidizer mixtures or hot combustion products are quenched or cooled by the walls, respectively. Both effects represent physics that are distinct from those embedded in the flamelet equations and therefore challenging to incorporate into the model.

Finally, the range of flamelet equation boundary conditions for the HDCR was quantified by plotting the PDFs of the pressure and temperature for the pure fuel and oxidizer streams. It should be noted that, although the oxidizer stream pressures are close to the combustor pressure, the fuel stream pressures are independent and a function of only the scramjet fuel injection system design, particularly whether the fuel streams are overexpanded, underexpanded, or pressure matched. If the injection pressure is pressure matched to the combustor, then parameterizing the flamelet using the combustor pressure offers a reasonable approach. However, even under the pressure matched injection conditions, the static temperature of the fuel and oxidizer streams will vary and therefore require further parameterization. Furthermore, these temperature differences will be due to completely different physical processes, i.e., shock train processes due to combustor back-pressuring for the oxidizer stream, and fuel injection system design and total temperature of the fuel (which may have been heated) when entering the combustor. Similar to the challenges associated with parameterizing the heat transfer, parameterizing the boundary condition effects is a nontrivial task.

Some of the challenges with using steady flamelet models for applications in supersonic combustion may be reduced or eliminated by using the unsteady flamelet [28] or representative interactive flamelet [30] approaches, albeit at the expense of higher computational cost. However, given the number of approximations and parameterizations needed to address all of the above issues, while still being constrained by the flamelet thin flame approximation and the fact that at least one non-flamelet simulation would generally be needed to provide information about the pressure range and the boundary conditions for the flamelet equations, it might be reasonable to revert to an alternate strategy, such as the optimized global reaction mechanisms [100], or specially tuned eddy dissipation concept models [101]. Although the fidelity to accurately represent the chemical kinetics would be diminished and the production of some minor species of interest would not be available, these simpler models may be sufficient for many practical applications and are simpler to implement and use. To fully take advantage of the benefits of flamelet models for supersonic combustion, further research is needed to overcome the challenges discussed in this work.

References

1. W.H. Heiser, D.T. Pratt, *Hypersonic Airbreathing Propulsion* (AIAA, Washington, DC, 1994)
2. T. Poinsot, D. Veynante, *Theoretical and Numerical Combustion*, 2nd edn. (R.T. Edwards, Inc., Philadelphia, PA, 2005)
3. M. Conaire, H.J. Curran, J.M. Simmie, W.J. Pitz, C. Westbrook, A comprehensive modeling study of hydrogen oxidation. Int. J. Chem. Kinet. **36**(11), 603–622 (2004)
4. D.C. Wilcox, *Turbulence Modeling for CFD* (DCW Industries Inc, La Cañada, CA, 2006)
5. T. Lu, C. Law, Toward accommodating realistic fuel chemistry in large-scale computations. Prog. Energy Combust. Sci. **35**(2), 192–215 (2009)
6. R.J. Kee, M.E. Coltrin, P. Glarborg, Chemically reacting flow: theory and practice. Technical Report SAND2001-0143P (Sandia National Laboratories, Albuquerque, NM, 2001)
7. D.G. Goodwin, R.L. Speth, H.K. Moffat, B.W. Weber, Cantera: An object-oriented software toolkit for chemical kinetics, thermodynamics, and transport processes (2018). https://www.cantera.org. Version 2.4.0
8. K. Seshadri, F.A. Williams, Reduced chemical systems and their applications in turbulent combustion, in *Turbulent Reacting Flows*, ed. by P.A. Libby, F.A. Williams, Chap. 4, pp. 154–210 (Academic Press, London, UK, 1994)
9. B. Franzelli, E. Riber, M. Sanjosé, T. Poinsot, A two-step chemical scheme for kerosene-air premixed flames. Combust. Flame **157**, 1364–1373 (2010)
10. B.F. Magnussen, B.H. Hjertager, On mathematical modeling of turbulent combustion with special emphasis on soot formation and combustion, Proc. Combust. Inst. **16**(1), 719–729 (1977)
11. G. Esposito, M. Rahimi, H. Chelliah, V. Hiremath, S. Pope, D. Sheen, W. Tsang, Chemical kinetic model reduction and efficient implementation strategies for hypersonic propulsion applications, in *50th AIAA Aerospace Sciences Meeting Including the New Horizons Forum and Aerospace Exposition*, AIAA-2012-118 (AIAA, Nashville, TN, 2012)
12. N. Peters, Laminar diffusion flamelet models in non-premixed turbulent combustion. Prog. Energy Combust. Sci. **10**(3), 319–339 (1984)
13. N. Peters, Laminar flamelet concepts in turbulent combustion. Proc. Combust. Inst. **21**, 1231–1250 (1986)
14. N. Peters, *Turbulent Combustion* (Cambridge University Press, Cambridge Monographs on Mechanics, 2000)
15. F.A. Williams, Recent advances in theoretical description of turbulent diffusion flames, in *Turbulence in Mixing Operations*, ed. by R.S. Brodkey, pp. 189–209 (Academic Press, New York, 1975)
16. R.W. Bilger, The structure of diffusion flames. Combust. Sci. Technol. **13**, 155–170 (1976)
17. G. Dixon-Lewis, Structure of laminar flames, Proc. Combust. Ins. **23**(1), 305–324 (1991)
18. J. Larsson, I. Bermejo-Moreno, J. Bodart, R. Vicquelin, Predicting the operability limit of the HyShot II scramjet using LES, in *Center for Turbulence Research Annual Research Briefs* (2012)
19. J. Larsson, S. Laurence, I. Bermejo-Moreno, J. Bodart, S. Karl, R. Vicquelin, Incipient thermal choking and stable shock-train formation in the heat-release region of a scramjet combustor. Part II: large eddy simulations. Combust. Flame **162**(4), 907–920 (2015)

20. A.A.V. Perpignan, M.G. Talboom, Y. Levy, A.G. Rao, Emission modeling of an interturbine burner based on flameless combustion. Energy Fuels **32**, 822–838 (2018)
21. S. Pope, Computationally efficient implementation of combustion chemistry using in situ adaptive tabulation. Combust. Theor. Model. **1**, 41–63 (1997)
22. E.E. O'Brien, The probability density function (PDF) approach to reacting turbulent flows, in *Turbulent Reacting Flows*, ed. by P.A. Libby, F.A. Williams, vol. 44 of Topics in Applied Physics, Chap. 5, pp. 185–218 (Springer, Heidelberg, Germany, 1980)
23. R.L. Gaffney, J.A. White, S.S. Girimaji, J.P. Drummond, Modeling of turbulent/chemistry interactions using assumed PDF methods, in *28th AIAA/SAE/ASME/ASEE Joint Propulsion Conference and Exhibit*, AIAA-92-3638 (AIAA, Nashville, TN, 1992)
24. R.A. Baurle, G.A. Alexopoulos, H.A. Hassan, J.P. Drummond, An assumed joint-beta PDF approach for supersonic turbulent combustion, in *28th AIAA/SAE/ASME/ASEE Joint Propulsion Conference and Exhibit*, AIAA-92-3844 (AIAA, Nashville, TN, 1992)
25. S.H. Frankel, V. Adumitroaie, C.K. Madnia, P. Givi, Large eddy simulations of turbulent reacting flows by assumed PDF methods, in *Engineering Applications of Large Eddy Simulations*, ed. by S.A. Ragab, U. Piomelli, vol. 162, pp. 81–101 (ASME, Fluids Engineering Division, New York, 1993)
26. C.D. Pierce, Progress-variable approach for large eddy simulation of turbulent combustion. Ph.D. thesis, Stanford University, 2001
27. M. Ihme, L. Shunn, J. Zhang, Regularization of reaction progress variable for application to flamelet-based combustion models. J. Comput. Phys. **231**, 7715–7721 (2012)
28. M. Ihme, Y. Chee See, Prediction of autoignition in a lifted methane/air flame using an unsteady flamelet/progress variable model, Combust. Flame **157**, 1850–1862 (2010)
29. H. Pitsch, M. Chen, N. Peters, Unsteady flamelet modeling of turbulent hydrogen-air diffusion flames, Proc. Combust. Ins. **27**(1), 1057–1064 (1998)
30. S.-H. Keum, An improved representative interactive flamelet model accounting for evaporation effect in reaction space. Ph.D. thesis, University of Michigan, 2009
31. C.D. Pierce, P. Moin, Progress-variable approach for large-eddy simulation of non-premixed turbulent combustion. J. Fluid Mech. **504**, 73–97 (2004)
32. M. Ihme, C.M. Cha, H. Pitsch, Prediction of local extinction and re-ignition effects in non-premixed turbulent combustion using a flamelet/progress variable approach. Proc. Combust. Inst. **30**(1), 793–800 (2005)
33. J. van Oijen, L. de Goey, Modeling of premixed laminar flames using flamelet-generated manifolds. Combust. Sci. Technol. **161**, 113–137 (2000)
34. J.A. van Oijen, *Flamelet-generated manifolds: development and application to premixed laminar flames*. Ph.D. thesis, Eidenhoven Technical University, Eidenhoven, Netherlands, 2002
35. J.A. van Oijen, A. Donini, R.J.M. Bastiaans, J.H.M. ten Thije Boonkkamp, L.P.H. de Goey, State-of-the-art in premixed combustion modeling using flamelet generated manifolds. Prog. Energy Combust. Sci. **57**, 30–74 (2016)
36. N. Hass, K. Cabell, A. Storch, HIFiRE direct-connect rig (HDCR) phase I ground test results from the NASA Langley arc-heated scramjet test facility, in *JANNAF* (2010)
37. A. Storch, M. Bynum, J. Liu, M. Gruber, Combustor operability and performance verification for HIFiRE flight 2, in *17th AIAA International Space Planes and Hypersonic Systems and Technologies Conference* (San Francisco, CA, 2011)
38. Z. Luo, C.S. Yoo, E.S. Richardson, J.H. Chen, C.K. Law, T.F. Lu, Chemical explosive mode analysis for a turbulent lifted ethylene jet flame in highly-heated coflow. Combust. Flame **159**(1), 265–274 (2012)
39. K. Cabell, N.E. Hass, A. Storch, M. Gruber, HIFiRE direct-connect rig (HDCR) phase I scramjet test results from the NASA Langley arc-heated scramjet test facility, in *17th AIAA International Space Planes and Hypersonic Systems and Technologies Conference* (San Francisco, CA, 2011)
40. R.L. Panton, *Incompressible Flow* (Wiley, New York, 1984)
41. F.A. Williams, *Combustion Theory*, 2nd edn. (The Benjamin/Cummings Publishing Company, Menlo Park, CA, 1985)

42. S.R. Turns, *An Introduction to Combustion: Concepts and Applications*, 2nd edn. (McGraw Hill, 2000)
43. K.K. Kuo, *Principles of Combustion* (Wiley, Hoboken, N.J., 2005)
44. J. Warnatz, U. Maas, R.W. Dibble, *Combustion*, 4th edn. (Springer, Berlin, Germany, 2006)
45. C.K. Law, *Combustion Physics* (Cambridge University Press, 2006)
46. P. Gnoffo, R.N. Gupta, J.L. Shinn, *Conservation equations and physical modes for hypersonic air flows in thermal and chemical nonequilibrium, NASA Technical Paper 2867* (NASA, Hampton, VA, 1989)
47. C. Park, *Nonequilibrium Hypersonic Aerothermodynamics* (Wiley, New York, 1990)
48. G.M. Faeth, Evaporation and combustion in sprays. Prog. Energy Combust. Sci. **9**, 1–76 (1983)
49. J.P. Drummond, Supersonic reacting internal flow fields, in *Numerical Approaches to Combustion Modeling*, ed. by E.S. Oran, J.P. Boris, vol. 135 of Progress in Astronautics and Aeronautics, Chap. 12, pp. 365–420 (AIAA, Washington, D.C., 1991)
50. M. Safari, M.R.H. Sheikhi, M. Janbozorgi, H. Metghalchi, Entropy transport equation in large eddy simulation for exergy analysis of turbulent combustion systems. Entropy **12**(3), 434–444 (2010)
51. H. Tennekes, J.L. Lumley, *A First Course in Turbulence* (MIT Press, Cambridge, MA, 1972)
52. J.O. Hinze, *Turbulence* (McGraw Hill Book Company, New York, 1975)
53. P.A. Libby, F.A. Williams (eds.), *Turbulent Reacting Flows* (Academic Press, London, UK, 1994)
54. S.B. Pope, *Turbulent Flows* (Cambridge University Press, Cambridge, UK, 2000)
55. K.A. Hoffmann, S.T. Chiang, *Computational Fluid Dynamics*, vol. 1, 4th edn. (Engineering Education Systems, Wichita, KS, 2000)
56. K.A. Hoffmann, S.T. Chiang, *Computational Fluid Dynamics*, vol 2, 4th edn. (Endingeering Education System, Wichita, KS, 2000)
57. J.H. Ferziger, M. Perić, *Computational Methods for Fluid Mechanics*, 3rd edn. (Springer, Berlin, Germany, 2002)
58. J. Blazek, *Computational Fluid Dynamics: Principles and Applications*, 2nd edn. (Elsevier, Washington, D.C., 2005)
59. K. Masatsuka, *I Do Like CFD*, vol. 1, 2nd edn. (2013). http://www.cfdbooks.com/cfdbooks.html
60. R.H. Pletcher, J.C. Tannehill, D.A. Anderson, *Computational Fluid Mechanics and Heat Transfer*, 3rd edn. (CRC Press, Boca Raton, FL, 2013)
61. K.A. Hoffmann, S.T. Chiang, *Computational Fluid Dynamics*, vol. 3, 4th edn. (Engineering Education System, Wichita, KS, 2000)
62. D.C. Wilcox, *Turbulence Modeling for CFD* (DCW Industries Inc, La Cañada, CA, 2000)
63. P. Sagaut, *Large Eddy Simulation of Incompressible Flows: An Introduction*, 3rd edn. (Springer, Berlin, Germany, 2006)
64. E. Garnier, N. Adams, P. Sagaut, *Large Eddy Simulation for Compressible Flows* (Springer, Netherlands, 2009)
65. P.A. Durbin, B.A.P. Reif, *Statistical Theory and Modeling for Turbulent Flows*, 2nd edn. (Wiley Ltd., New York, 2011)
66. G.I. Taylor, Statistical theory of turbulence. Proc. Royal Soc. (A) **151**, 421–478 (1935)
67. R.A. Baurle, Modeling of high speed reacting flows: Established practices and future challenges, in *42nd AIAA Aerospace Sciences Meeting and Exhibit*, AIAA-2004-267 (AIAA, Reno, NV, 2004)
68. R.W. Bilger, S.H. Starner, R.J. Kee, On reduced mechanisms for methane-air combustion in nonpremixed flames. Combust. Flame **80**, 135–149 (1990)
69. R.S. Barlow, J.H. Frank, Effects of turbulence on species mass fractions in methane/air jet flames. Proc. Combust. Inst. **27**, 1087–1095 (1998)
70. H. Pitsch, N. Peters, A consistent flamelet formulation for non-premixed combustion considering differential diffusion effects. Combust. Flame **114**, 26–40 (1998)
71. T.F.C. Chan, H.B. Keller, Arc-length continuation and multi-grid techniques for nonlinear elliptic eigenvalue problems. SIAM J. Sci. Stat. Comput. **3**(2), 173–194 (1982)

72. H.F. Mrema, G.V. Candler, Large eddy simulation of supersonic combustion using the flamelet/progress-variable approach and the evolution-variable manifold approach, in *AIAA Scitech Forum* (San Diego, CA, 2019)
73. J. Urzay, Supersonic combustion in air-breathing propulsion systems for hypersonic flight. Ann. Rev. Fluid Mech. **50**, 593–627 (2018)
74. G.L. Brown, A. Roshko, On density effects and large structure in turbulent mixing layers. J. Fluid Mech. **64**, 775–816 (1974)
75. D.W. Bogdanoff, Compressibility effects in turbulent shear layers. AIAA J. **21**(6), 926–927 (1983)
76. D. Papamoschou, A. Roshko, The compressible turbulent shear layer: an experimental study. J. Fluid Mech. **197**, 453–477 (1988)
77. H. Foysi, S. Sarkar, The compressible mixing layer: An LES study. Theor. Comp. Fluid. Dyn. **24**, 565–588 (2010)
78. M. Oevermann, Numerical investigation of turbulent hydrogen combustion in a SCRAMJET using flamelet modeling. Aerosp. Sci. Technol. **4**, 463–480 (2000)
79. V.E. Terrapon, F. Ham, R. Pecnik, H. Pitsch, A flamelet-based model for supersonic combustion, in *Center for Turbulence Research Annual Research Briefs* (2009)
80. A. Saghafian, V.E. Terrapon, H. Pitsch, An efficient flamelet-based combustion model for compressible flows. Combust. Flame **162**(3), 652–667 (2015)
81. R. Pecnik, V. Terrapon, F. Ham, G. Iaccarino, H. Pitsch, Reynolds-averaged Navier Stokes simulations of the HyShot II scramjet. AIAA J. **50**, 1717–1732 (2012)
82. J.R. Quinlan, Flamelet/progress variable modeling for a dual-mode scramjet combustor. Ph.D. thesis, University of Virginia, Charlottesville, VA, 2015
83. P.G. Ferlemann, Forebody and inlet design for the HIFiRE 2 flight test, in *JANNAF Airbreathing Propulsion Subcommittee Meeting* (Boston, MA, 2008)
84. G.L. Pellett, S.N. Vaden, L.G. Wilson, Gaseous surrogate hydrocarbons for a HIFiRE scramjet that mimic opposed jet extinction limits for cracked JP fuels, in *55th JANNAF Propulsion Meeting, NTRS Report Number 20080020388* (Boston, MA, 2008)
85. Viscous Upwind ALgorithm for Complex Flow ANalysis (VULCAN): User manual (2010)
86. D.C. Wilcox, Wall matching, a rational alternative to wall functions, in *27th Aerospace Sciences Meeting* (Reno, NV, 1989)
87. V. Cuda, N.E. Hass, Heat flux and wall temperature estimates for the NASA Langley HIFiRE direct connect rig, in *JANNAF 43rd CS/31st APS/25th PSHS Joint Subcommittee Meeting* (La Jolla, CA, 2009)
88. F.R. Menter, Two-equation eddy-viscosity turbulence models for engineering applications. AIAA J. **32**, 1598–1605 (1994)
89. J.R. Edwards, A low-diffusion flux-splitting scheme for Navier-Stokes calculations. Comput. Fluids. **26**, 635–659 (1997)
90. T.H. Pulliam, D.S. Chaussee, A diagonal form of an implicit approximate-factorization algorithm. J. Comput. Phys. **39**, 347–363 (1981)
91. R. Baurle, Analysis of facility non-equilibrium thermodynamic effects on HIFiRE ground tests, in *JANNAF 46th CS/34th APS/34th EPSS/28th PSHS Joint Subcommittee Meeting* (Albuquerque, NM, 2014)
92. G. Lacaze, E. Richardson, T. Poinsot, Large eddy simulation of spark ignition in a turbulent methane jet. Combust. Flame **156**, 1993–2009 (2009)
93. H. Yamashita, M. Shimada, T. Takeno, A numerical study on flame stability at the transition point of jet diffusion flames. Proc. Combust. Inst. **26**, 27–34 (1996)
94. E. Sozer, E. Hassan, S. Yun, S. Thakur, J. Wright, M. Ihme, W. Shyy, Turbulence-chemistry interaction and heat transfer modeling of H2/O2 gaseous injector flows, in *48th AIAA Aerospace Sciences Meeting and Exhibit* (Orlando, FL, 2010)
95. D.J. Lee, M. Ihme, S. Thakur, W. Shyy, LES of a gaseous H2/O2 rocket injector: wall heat transfer modeling, in *13th International Conference on Numerical Combustion* (Corfu, Greece, 2011)

96. H. Wu, M. Ihme, Modeling of unsteady heat transfer in flame-wall interaction, in *66th Division of Fluid Dynamics Meeting of the American Physical Society* (Pittsburgh, PA, 2013)

97. P.C. Ma, H. Wu, M. Ihme, J.-P. Hickey, Nonadiabatic flamelet formulation for predicting wall heat transfer in rocket engines. AIAA J. **56**(6), 2336–2349 (2018)

98. H. Barths, C. Hasse, G. Bikas, N. Peters, Simulation of combustion in direct injection diesel engines using an Eulerian particle flamelet model. Proc. Combust. Inst. **28**(1), 1161–1167 (2000)

99. C. Felsch, M. Gauding, C. Hasse, S. Vogel, N. Peters, An extended flamelet model for multiple injections in DI diesel engines. Proc. Combust. Inst. **32**(1), 2775–2783 (2009)

100. C.K. Westbrook, F.L. Dryer, Simplified reaction mechanisms for oxidation of hydrocarbon fuels in flames. Combust. Sci. Technol. **27**, 31–43 (1981)

101. A.T. Norris, Tuning process for the modified Magnussen combustion model, in *AIAA Propulsion and Energy Forum* (Cincinnati, OH, 2018)